



## Bed-flow instability of the longshore current

A. FALQUÉS,\* A. MONTOTO† and V. IRANZO\*

(Received 8 July 1994; in revised form 25 May 1995; accepted 16 October 1996)

**Abstract**—An initially uniform longshore current on a plane erodible beach is considered and a linear stability analysis of the bed-flow system is performed in order to investigate the growth of alongshore periodic topographic features such as transverse or oblique bars. A numerical model based on the shallow water equations and a simple sediment transport formula is used. For a wide range of parameters instability is found, leading to the growth of large-scale topographic features (lengthscale of the order of the current width) downflow progressing. The growth rates and the dominant unstable mode depend mainly on  $R = c_b/\beta$  parameter, where  $c_b$  is the bottom friction coefficient and  $\beta$  is the beach slope. For a small  $R$ , say less than 0.1, instability is very weak, probably negligible. For  $R$  between 0.1 and 0.7 instability increases with  $R$ , leading typically to a quite simple transverse bars pattern. A further increase in  $R$  produces a far more complicated behaviour where complex patterns with downcurrent oriented oblique bars, bumps and holes can be dominant. In this region growth rates may either decrease or increase with  $R$  depending on the beach slope and the maximum Froude number of the basic flow,  $F$ . Usually, the most complex behaviour is found for gently sloping beaches. The physical mechanism of the instability is found to lie on the disturbances of potential vorticity caused by topographically induced differences in bottom friction. In this sense it is similar to the alternate bars growth in a river rather than the dunes or antidunes occurrence for 1D channel flow. The predictions of the model compare well with the available experimental data. The alongshore wavelength,  $\lambda$ , typically of the order of one to four times the width of the current, is close to four times for the most common values of  $R$ . The typical growth time is proportional to  $\lambda^2$  and for a wavelength of 100 m can be of the order of one day, depending on the sediment transport rate. The migrational speed is inversely proportional to  $\lambda$ , in accordance to earlier field data reported by Sonu [(1969) Collective movement of sediment in littoral environment. *Proceedings of the 11th International Conference on Coastal Engineering, A.S.C.E.*, New York.]. Copyright © 1996 Elsevier Science Ltd

### 1. INTRODUCTION

Coastal morphodynamics lies on a number of complex multi-scale nonlinear processes which involve waves, currents and sediment transport in interaction with the changing topography. Even when the vertical structure of the flow is ignored and the short wave input is parameterized by using depth and wave period averaged equations a highly complex dynamical behaviour still remains on the lengthscale of the surf zone width and the timescale of infragravity motions [ $O(50$  s)] or larger. In the most idealized situation,

---

\*Department of Applied Physics, Universitat Politècnica de Catalunya, 08034 Barcelona, Spain.

†Department of Physics and Nuclear Engineering, Universitat Politècnica de Catalunya, 08034 Barcelona, Spain.

i.e. waves incoming on a long, straight beach with alongshore uniformity, simple equilibrium solutions of the governing equations exist. When waves approach the shore normally, a setup/setdown of the mean water level without mean motion provides this equilibrium. For obliquely incident waves a longshore current with alongshore uniformity also results to achieve equilibrium. This simple equilibrium between wave forcing, pressure gradients and frictional forces is widely used by coastal scientists and engineers to predict currents, sediment transport and thereby shore evolution. However, these simple steady and alongshore uniform solutions very often break down into complex patterns with more or less alongshore regularity. These patterns may exist in the water motions within the surf/shoaling zone as horizontal circulation cells or eddies, rip currents, meandering in the longshore current, progressing or standing edge waves, etc. However, they can also exist, sometimes in a striking way, in the shoreline morphology and in the surf zone topography as beach cusps, transverse/oblique bars, crescentic longshore bars, ridge and runnel systems, etc. These morphological features, usually known in a broad sense as rhythmic topography, should obviously be coupled with correlated hydrodynamic patterns, especially at the moment of their formation. The contrary is not so evident, as many time dependent flow patterns may not have a counterpart in the topography.

Many different physical mechanisms have been proposed to explain this complicated hydrodynamic and morphodynamic behaviour. One possibility is the existence of slow temporal or spatial modulations in the external forcing. Bowen (1969) showed how a small longshore periodic variation in the incoming wave amplitude can induce rip currents and horizontal eddies. These alongshore variations can be provided by intersecting wave trains (Dalrymple, 1975) or by standing edge waves (Bowen and Inman, 1969). In both cases the residual circulation can generate morphological features like beach cusps and crescentic longshore bars (Dalrymple and Lanan, 1976; Bowen and Inman, 1971). Following this course of thinking, the interaction of two edge wave modes of the same frequency but different wavelength may also give rise to rhythmic topography in some cases highly reminiscent of observed oblique bar systems (Holman and Bowen, 1982). But the question arises of whether edge waves are actually present in the surf zone and how they can be generated. Some researchers have shown that infragravity edge waves can be excited by a temporal modulation of the incoming wave groups (Schäffer, 1994). Moreover, field observations of the occurrence of edge waves and of their link to beach morphology has already been well documented (see, for instance, Bowen and Huntley, 1984; Wright *et al.*, 1986; Bauer and Greenwood, 1990).

On the other hand, nearshore large scale complex dynamics have been observed even in the absence of any modulation in the external forcing. Thereby, much research has focused on mechanisms based on the inherent behaviour of the coastal dynamical system through free instabilities of the basic steady equilibrium. These instability mechanisms may be either purely hydrodynamic—that is, those that can take place even on a non-erodible bottom—or morphodynamic, those essentially based on sediment transport through a positive feedback between bed perturbations and flow perturbations. The edge wave excitation by wave-wave interaction in the nearshore is one example of the former type (Guza and Bowen, 1975). It provides an explanation for edge wave generation without any inhomogeneity in the external forcing that was observed in laboratory beaches by Bowen and Inman (1969). Another source of hydrodynamic instability that can yield steady equilibrium solutions different from the simplest one is the potential energy stored by the setup/setdown (Miller and Barcilon, 1978). A third example is the instability driven

by the cross-shore shear in the longshore current which, according to Bowen and Holman (1989), gives an explanation for the so-called "shear or vorticity waves" first observed by Oltman-Shay *et al.* (1989). Shear waves are large-scale [ $O(100\text{ m})$ ] eddies which progress downcurrent and produce a meandering in the longshore current with periods [ $O(100\text{ s})$ ] much longer than the possible gravity modes of the same wavelength. They have been extensively investigated in the last few years (see, for instance, Falqués and Iranzo, 1994) and have recently been generated in a laboratory beach by Reniers *et al.* (submitted).

Any of the above-mentioned hydrodynamic processes can generate sedimentary patterns in the nearshore. However, this can also be accomplished by specifically morphodynamic instability mechanisms. As early as 1969, Sonu hypothesized that the "interaction between longshore currents and an erodible bed" was a driving mechanism for cusp-type sand waves in a similar way to dune growth in the bed of a river. We will refer to this mechanism as "bed-flow instability". But when applied specifically to the surf zone this mechanism is usually linked to other processes directly related to the incoming wave field. As soon as a bed perturbation develops, a perturbation in the wave field and thereby a perturbation in the radiation stress result, which modifies the circulation pattern. If again a positive feedback between bedform growth and flow disturbance occurs, an instability of the system will result. The latter mechanism is conceptually different from the former one and we will refer to it as "bed-surf instability". A first description of it may be found in Niedoroda and Tanner (1970). Bed-flow instability is directly related to the longshore current and may act both in river and shore environments, whereas bed-surf instability may occur only in the surf zone. For oblique wave incidence both processes will coexist, whereas for normal incidence only bed-surf instability is possible.

Hino (1975) first investigated theoretically the instability driven by an incoming wave field on the surf zone bed-fluid system. He considered the shallow water equations for mass, momentum and sediment conservation in combination with a simple transport formula as governing equations. His model predicts the growth of longshore rhythmic patterns linked to horizontal circulation cells and/or meandering in the longshore current. The model leads to a dominant wavelength, that is, a fastest growing wavelength,  $\lambda \approx 4X_b$  where  $X_b$  is the surf zone width. According to Hino, there are two instability sources in his model: the "sand wave formation" (i.e. bed-flow instability) and wave setup. Nevertheless, it is obvious from his formulation that the bed-surf mechanism is also present. Hydrodynamic instabilities like shear wave or edge wave generations are filtered out by the quasi-steady assumption—that is, the flow adjusts instantaneously to a slow varying topography. The work of Hino has recently been extended by Christensen *et al.* (1995), who have considered several sand transport models and irregular waves instead of regular waves. Their results are partially in contrast with Hino's results. For instance, in the case of a sand transport which is proportional to the velocity (as in Hino) no dominant wavelength is obtained. For more sophisticated transport models a dominant wavelength  $\lambda \approx 6X_b$  is found. The orientation of the growing oblique bars depends strongly on the gradient in the longshore current profile and may be upflow skewed.

Hino's model includes both mechanisms (bed-flow and bed-surf), and it is obvious that both will usually operate in natural beaches. In addition, not only these two processes but also many others like edge wave generation, shear instabilities or modulation in the external forcing may occur simultaneously, some of them prevailing in some beach and weather conditions and some of them in others. Therefore, as a preliminary step towards

more in-depth study, each mechanism should be investigated in isolation. For oblique wave incidence, an alongshore migration of sand waves is very often observed (Sonu, 1973; Hunter *et al.*, 1979). This suggests that the physical processes involved in bed-flow instability are very common. However, the question arises of: (1) whether the bed-flow interaction results in a positive feedback leading to the growth of patterns rather than just a migration of pre-existing features; and (2) which mechanisms prevail in each real situation and what the experimental implications are. The purpose of this paper is to provide a theoretical analysis of the bed-flow instability mechanism in isolation so as to address the first item. Although a thorough examination of the second item is beyond the scope of the present paper, some discussion and comparison with observed rhythmic topography will be included. In addition to the above-mentioned reasons, bed-flow instability is worth investigating because the strong dependence of bar orientation on the shear in the current found by Christensen *et al.* (1995) suggests that the influence of the longshore current alone can be very significant. Furthermore, the low resolution of Hino's numerical model and the fact that it is partially subject to discussion recommend such a detailed analysis of each "ingredient".

Even though the bed-flow instability mechanism was already suggested by Sonu (1969), it has been paid little attention. Barçilon and Lau (1973) proposed a model for the formation of transverse bars on low energy beaches. Their analysis is mainly aimed at longshore currents driven by tides, river discharge or wind rather than waves and may be considered the first theoretical study of bed-flow instability in the nearshore. They considered an erodible plane beach drift by a longshore current without cross-shore gradient. Potential flow and a simple sediment transport formula was assumed, and a linear stability analysis was performed. The dominant instability mode for the bed-fluid system proved to be quite similar to the wavelength of some transverse bar families in several low energy beaches. However, an important theoretical drawback was found in this approach (Falqués, 1991). The model was reconsidered and proved to yield a characteristic spacing of the bars related to steady edge waves, i.e. steady flows stemming from an upstream edge wave held stationary by the current. This characteristic spacing is

$$\lambda = 2\pi \frac{V^2}{g\beta} \quad (1)$$

where  $V$  is the longshore current and  $\beta$  the beach slope. The presence of steady edge waves was further investigated for longshore currents with cross-shore variation (Falqués *et al.*, 1993), and it was shown that the existence of the characteristic wavelength given by equation (1) for the Barçilon and Lau model was due to the fact that the maximum Froude number of the basic flow was larger than 1, a condition hardly realistic for natural beaches. Therefore, the aim of the present paper is to extend the above-mentioned research by: (1) considering a more realistic longshore current profile; (2) introducing bottom friction; (3) relaxing the potential flow assumption; and (4) removing the hypothesis of a lag distance between flow and sediment transport taken into account by Barçilon and Lau.

We consider a basic current profile aimed at wave driven flows in the surf zone. However, the numerical model could be readily applied to other environmental conditions just by selecting a suitable basic current and topography. We use the shallow water equations with a quadratic bottom friction and a driving term which may be radiation stresses or some other source. A sediment conservation equation is considered in combination with a simple transport model based on a sediment flux which is some power

of the current. The model is described in Section 2. As a basic undisturbed state we assume a plane sloping beach with a rectilinear shoreline and a longshore current which is alongshore uniform but with cross-shore shear. Then, a linear stability analysis is performed by means of numerical simulation (Section 3). We obtain the dispersion relations of the unstable modes and their growth rates as a function of their wavelength. Some attention is also paid to the spatial pattern of the growing bedforms. Section 4 is devoted to gaining insight into the physical mechanism of the instability. In Section 5 some discussion, including comparison with other theoretical models and with observed rhythmic beach features and rip current systems, is presented. Section 6 ends with a brief summary of our conclusions. An appendix on the numerical method is also included.

## 2. THE MODEL

We consider an erodible beach drift by a longshore current. In the basic undisturbed state the shoreline is rectilinear and the beach and the flow are assumed to be alongshore uniform. As shown in Fig. 1, we use an orthogonal coordinate system with  $x$  cross-shore,  $y$  running alongshore and  $z$  vertically upwards. The fluid motions are considered to be governed by the shallow water equations (depth averaged momentum equations and mass conservation equation)

$$\frac{\partial \vec{V}}{\partial t} + (\vec{V} \cdot \nabla) \vec{V} + \mathbf{g} \nabla (z_b + \xi) = \vec{\mathcal{F}} - \frac{c_d}{\xi} |\vec{V}| \vec{V} \quad (2)$$

$$\frac{\partial \xi}{\partial t} + \nabla \cdot (\xi \vec{V}) = 0 \quad (3)$$

where  $\xi(x, y, t)$  is the total depth and  $z = z_b(x, y, t)$  is the level of the bottom. In (2) – (3)  $\Delta$  stands for  $(\partial_x, \partial_y)$ ,  $\vec{V}$   $\mathcal{F}$  is the horizontal depth averaged velocity of the fluid,  $c_d$  is a drag coefficient for bottom friction and  $\mathcal{F}$  stands for the forcing terms. These terms may be due to radiation stresses or to other energy sources. In the former case, we have

$$\vec{\mathcal{F}} = -\frac{1}{\xi} \nabla \cdot S. \quad (4)$$

These equations are time averaged over a time period longer than the period of wind or swell waves. Coriolis terms and lateral momentum diffusion have both been neglected. If our model is applied only to the nearshore region, Coriolis terms might be negligible. Instead, any extension to a larger scale region should take these terms into account. According to the work by Schielen *et al.* (1993) (hereafter SDS93), which deals with a very similar mathematical model but aimed at a fluvial environment, bottom friction is essential in order for bed-flow instabilities to develop. For this reason we take bottom friction into account, whereas we neglect turbulent eddy viscosity, which seems to play only a secondary role.

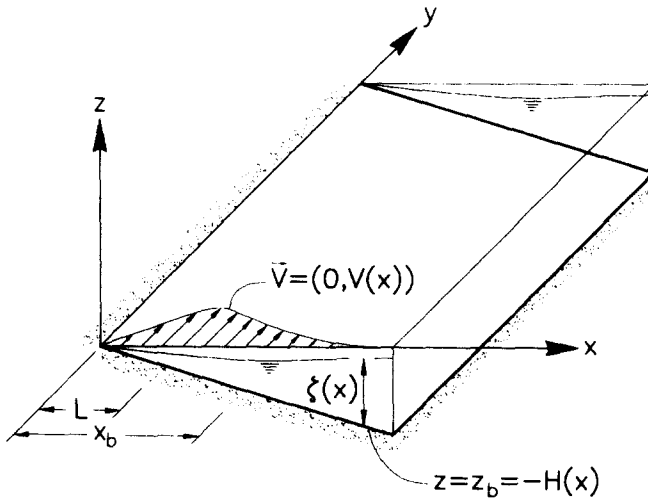
Sediment transport is a very complicated matter, especially in the surf zone (see van Rijn, 1989, for a review). However, we think that hydrodynamics plays a dominant role in such a way that an accurate description of sediment transport is not necessary for an initial approach to the morphological instabilities we are dealing with. Furthermore, our aim is to

keep our model as simple as possible, in order to give some conceptual insight into the basic physical mechanism. Thus, we consider a sediment conservation equation

$$\frac{\partial z_b}{\partial t} + \nabla \cdot \vec{q} = 0 \tag{5}$$

where  $\vec{q}(x,y,t)$  stands for the volumetric sediment flux, in combination with a simple standard law

Undisturbed state



Perturbed state

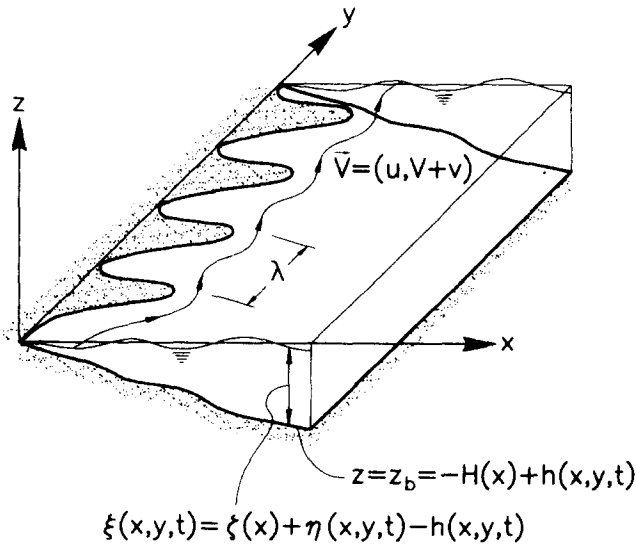


Fig. 1. Sketch of the flow, bedforms, physical parameters and coordinate system.

$$\vec{q} = v(|\vec{V}| - V_c)^m \left( \frac{\vec{V}}{|\vec{V}|} - \gamma \nabla h \right) \quad \text{if } |\vec{V}| > V_c \quad (6)$$

and  $\vec{q} = 0$  if  $|\vec{V}| < V_c$ . This procedure is very similar to the approach in SDS93, except for the inclusion of a threshold velocity,  $V_c$ , below which there is no transport. Here,  $m \geq 2$  is some exponent and  $v$  is a proportionality constant which depends on the sediment properties. The term  $\gamma \Delta h$ , where  $h(x, y, t)$  is any perturbation of  $z_b$  from its equilibrium value, accounts for the tendency of sand to move downhill. This term should in principle be written as  $\gamma \Delta(z_b + h)$  but  $\gamma \Delta z_b$  is balanced in some way (for instance, by the mean inshore transport due to waves) so that  $z = z_b$  is an equilibrium bathymetry. The constant  $\gamma$  is related to the Coulomb friction and typical values are of the order of 1. Some further discussion and some references related to this transport model may be found in SDS93.

Let us now define a basic state from which bedforms will grow due to instability. Thus, consider a longshore flow given by:

$$\vec{V} = (0, V(x)), \quad \xi = \zeta(x) \quad (7)$$

on a beach given by:

$$z_b = -H(x). \quad (8)$$

We assume the still water level given by  $z = 0$ , so that the wave setup/setdown would be given by  $\zeta(x) - H(x)$ . In order for the flow given by equation (7) to be a solution of the governing equations (2)–(6) we assume

$$g \frac{d(\zeta - H)}{dx} = \mathcal{F}_x, \quad \frac{c_d V^2}{\zeta} = \mathcal{F}_y. \quad (9)$$

Regarding the basic current, a profile

$$V(x) = axe^{-bx} \quad (10)$$

has been considered, which is aimed at describing the longshore current due to incoming waves with an oblique incidence in the surf zone. A plane beach topography

$$H(x) = \beta x \quad (11)$$

has been assumed. These two simple analytical expressions provide us with insight into the basic physical processes avoiding unnecessary complications, but the model can be handled with any other profiles.

Let us now consider a small perturbation of the basic state:

$$\vec{V} = [0, V(x)] + [u(x, y, t), v(x, y, t)] \quad (12)$$

$$z_b = -H(x) + h(x, y, t), \quad \xi = \zeta(x) + \eta(x, y, t) - h(x, y, t) \quad (13)$$

where  $h$  is the perturbation of the bottom and  $\eta$  is the perturbation of the free surface. Furthermore, to deal with dimensionless magnitudes, we choose as velocity and length scales the maximum of the longshore current and the distance from the shoreline where it takes place, that is,  $U = a/be$  and  $L = b^{-1}$ .

Of course, even though our analytic basic current profile decreases to 0 far offshore, it does not exactly vanish. Nevertheless, for practical purposes we will assume a finite width of the surf zone of the order of twice the distance from the shoreline to the maximum in the

current, that is,  $X_b = 2L$ . A characteristic Froude number may be defined as  $f = U/\sqrt{g\beta L}$ , related to the maximum Froude number of the basic flow,  $F$ , by  $F = \sqrt{e/2f}$ . All the fluid velocities in the model are scaled to  $U$  and the remaining variables are scaled according to:

$$(x, y) = L(x', y'), \quad t = Tt' \quad (14)$$

$$\zeta = \beta L \zeta', \quad h = \beta L h', \quad \eta = \frac{U^2}{g} \eta' \quad (15)$$

where  $T$  is the morphological timescale which will be specified later. The next step is to linearize the governing equations (2)–(6), taking into account that the perturbations in equations (12) and (13) are small. After some standard calculations we obtain as linearized equations:

$$\frac{L}{UT} \frac{\partial u}{\partial t} + V \frac{\partial u}{\partial y} + \frac{\partial \eta}{\partial x} + \frac{c_d}{\beta} V \frac{u}{\zeta} = 0 \quad (16)$$

$$\frac{L}{UT} \frac{\partial v}{\partial t} + \frac{dV}{dx} u + V \frac{\partial v}{\partial y} + \frac{\partial \eta}{\partial y} + 2 \frac{c_d}{\beta} V \frac{v}{\zeta} - \frac{c_d}{\beta} \frac{V^2}{\zeta^2} (f^2 \eta - h) = 0 \quad (17)$$

$$\frac{L}{UT} \left( f^2 \frac{\partial \eta}{\partial t} - \frac{\partial h}{\partial t} \right) + \frac{\partial}{\partial x} (\zeta u) + \zeta \frac{\partial v}{\partial y} + V \left( f^2 \frac{\partial \eta}{\partial y} - \frac{\partial h}{\partial y} \right) = 0 \quad (18)$$

$$\frac{\beta L^2}{v T U^m} \frac{\partial h}{\partial t} + \frac{\partial q_x}{\partial x} + \frac{\partial q_y}{\partial y} = 0 \quad (19)$$

where

$$q_x = (V - V_c)^m \left( \frac{u}{V} - \beta \gamma \frac{\partial h}{\partial x} \right), \quad q_y = (V - V_c)^{m-1} \left[ m v - \beta \gamma (V - V_c) \frac{\partial h}{\partial y} \right] \quad (20)$$

if  $V \geq V_c$  and  $q_x = q_y = 0$  otherwise. The bars have been dropped from terms which involve  $c_d |V|$  and  $|V| - V_c$  because we are concerned with a basic current such that  $V(x) \geq 0$ . In the dimensionless velocity field,  $a$  has been replaced by  $e$  and  $b$  by 1. Note that any perturbation in the driving forces,  $\mathcal{F}$ , has been neglected. The reason for such an assumption is discussed later on, at the end of this section. Now, we choose the morphological timescale as the factor in the first term of equation (19), that is,  $T = \beta L^2 / v U^m$ . On the other hand,  $L/U$  defines a hydrodynamic timescale. Typical values of  $L$  and  $U$  in the field are 100 m and  $1 \text{ m s}^{-1}$  respectively, so that the order of magnitude of  $L/U$  is of about 2 min, whereas the morphological time may be 1 h or more. Laboratory values may be estimated from an experiment by Horikawa and Sasaki reported by Sonu (1973) where the growth of rhythmic topography under oblique waves was observed. In this case,  $L \sim 2 \text{ m}$ ,  $U \sim 0.3 \text{ m s}^{-1}$ , giving a hydrodynamic time scale of about 7 s, whereas the time for significant morphological changes could be estimated to be at least of 10 min. Therefore, we may assume  $L/UT \ll 1$ , which allows us to drop the time derivatives in equations (16)–(17)–(18). This quasi-steady hypothesis means that the fluid adjusts instantaneously to the bottom configuration all the time and is very common in morphodynamic models (see SDS93).

Now, we assume alongshore travelling wave solutions and we therefore assume dependences in time and in the alongshore coordinate of the form:

$$(u, v, \eta, h) = [\hat{u}(x), \hat{v}(x), \hat{\eta}(x), \hat{h}(x)]e^{i(ky - \omega t)} \quad (21)$$

Thus,  $\lambda = 2\pi/k > 0$  will be the wavelength of the sand waves and  $\omega$  its complex frequency. The migration speed will be given by the phase velocity,  $c = \Re(\omega)/k = \omega_r/k$ , and  $\Im(\omega) = \omega_i$  will give the growth rate so that  $\omega_i > 0$  means instability and  $\omega_i < 0$  means stability. We also introduce the dimensionless parameter  $R = c_d/\beta$  and from equations (16) and (17) we obtain:

$$u = -\frac{1}{d_1} \frac{\partial \eta}{\partial x}, \quad v = \frac{1}{d_2} \left[ \frac{1}{d_1} \frac{dV}{dx} \frac{\partial \eta}{\partial x} + \left( Rf^2 \frac{V^2}{\zeta^2} - ik \right) \eta - R \frac{V^2}{\zeta^2} h \right] \quad (22)$$

with  $d_1 = ikV + RV/\zeta$  and  $d_2 = ikV + 2RV/\zeta$  and where hats have been dropped for convenience. Then, by substituting equation (22) in (19)–(20) and considering appropriate boundary conditions we finally obtain an eigenproblem

$$A(\eta, h) = i\omega B(\eta, h) \quad (23)$$

with the eigenvalue  $\omega$ , and the eigenfunction  $(\eta, h)$ . Here,  $A, B$  are two linear operators involving  $\partial_x$ . As boundary conditions at infinity we have considered that the perturbations vanish, i.e.

$$\eta(\infty) = 0, \quad h(\infty) = 0. \quad (24)$$

The shoreline,  $x = 0$ , is a singular point of the equations. A simple local analysis at this point shows that the regular solutions satisfy

$$\frac{\partial \eta}{\partial x}(0) = 0, \quad h(0) = 0 \quad (25)$$

so that equation (25) is an appropriate boundary condition at the shoreline. The physical meaning of this condition can be shown to be fluid and sediment conservation.

We have neglected any perturbation in the driving terms,  $\mathcal{F}$ . This assumption filters out the bed-surf instability included in Hino's model and quoted in Section 1. Furthermore, the setup/setdown have been neglected in the model calculations because once the perturbation in the forcing terms has been dropped the setup/setdown would add just a small correction on the basic total depth, which would be in turn equivalent to just a small deviation from the assumed planar topography. In fact, the setup could be incorporated in this planar bathymetry by a small correction on the slope,  $\beta$ , within the surf zone, and the setdown within the shoaling zone would result in a very small deviation from this planar topography (Horikawa, 1988). As will be seen, the model yields bedform growth only in the surf zone, so that the setdown is, indeed, negligible to our concern. Shear instabilities in the longshore current and the possible generation of edge waves have been filtered out by the quasi-steady hypothesis. Thus, only the bed-flow interaction has been selected as a single mechanism. It is worth noting that from a mathematical point of view our model is very close to the model in SDS93 for the formation of alternate bars in a channel. The only differences are (1) domain geometry: our "channel" has an infinite width and a transverse variation in depth; (2) basic flow: our basic flow has a transverse gradient; (3) free surface: we do not assume low Froude number (rigid lid); and (4) transport: we assume a threshold velocity for sediment transport. Thus, the present model may be considered as an extension of the model presented in SDS93 to more complex environmental conditions.

Therefore, the basic qualitative behaviour is expected to be essentially similar and the comparisons between the two models will be very helpful.

### 3. NUMERICAL SIMULATION

Equation (23) was solved numerically using rational Chebyshev expansions. A brief description of the method together with some useful references are presented in Appendix A. For each set of values of the parameters and for each wave number,  $k$ , solving the discrete version of equation (23) gives a spectrum of as many numerical eigenvalues  $\omega$  and eigenvectors  $(\eta, h)$  as the number of discretization points,  $N$ . These eigensolutions may be either approximations of true solutions of the original problem or spurious solutions, that is, solutions of the numerical problem that do not converge to proper solutions when  $N$  increases. Therefore, a convergence test on the numerical solutions for increasing  $N$  is necessary and we have only considered as reliable solutions those whose eigenvalue varies less than 5% when  $N$  increases from  $N_1$  to  $N_2$ . Usually,  $N_1 = 40$ ,  $N_2 = 60$  or  $N_1 = 60$ ,  $N_2 = 100$ . The rejected solutions may be either spurious ones or proper ones with too high a spatial complexity to be successfully described by the  $N = 40$  or  $N = 60$  meshes.

We have conducted an exploration for several values of the parameters  $R = c_d/\beta$  and  $\beta$  by fixing  $F = 0.1, 0.3, 0.5$ . Physically realistic values are:  $F \sim 0.0-0.5$ ,  $\beta \sim 0.001-0.05$  and  $c_d \sim 0.0005-0.02$  (see, for instance, Falqués *et al.*, 1995). Accordingly,  $R$  could range from 0.01 to 20. However, equilibrium beach profiles for coarse sand are steeper than profiles for finer sand, so that high values of the slope,  $\beta$ , will usually correspond to high values of the roughness and therefore, large values of  $c_d$ . As a result, the ratio  $R = c_d/\beta$  will not vary greatly, and typical values would range between 0.1 and 1. However, if small scale bedforms are present, or if the beach profile is above the equilibrium profile,  $R$  could be larger. On the other hand, a beach profile below the equilibrium profile would give smaller values of  $R$ , in such a way that high  $R$  would characterize accretion states and low  $R$  erosion states according to the nomenclature adopted by Wright and Short (1984). The power in the transport formula was always taken as  $m = 2$ , except for some particular tests where  $m = 1$  was considered. The threshold velocity for sand transport,  $V_c$ , was set at  $0.05U$  (except for a few tests with  $V_c = 0.1U, 0.5U, 0.8U$ ) and  $\gamma$  was fixed at 1. For each set of values of these parameters and for each  $k$  several reliable modes were found. The number of these solutions increases as the number of discretization nodes,  $N$ , increases. So, for each alongshore wave number,  $k$ , an infinite set of modes seems to exist. These modes will be numbered by  $n = 1, 2, 3, \dots$ . Mode 1 is the only reliable solution for a low mesh density, mode 2 the first appearing when the mesh density increases, mode 3 the second one and so on. As can be seen in Fig. 2 and similarly to SDS93, the mode number,  $n$ , is related to an increasing cross-shore spatial complexity. In dealing with numerical approximations, we have found the comparison with similar but simpler problems which can be solved analytically very helpful [see, for example, Bowen and Holman (1989) and Falqués and Iranzo (1994) on shear instability of longshore currents]. In the present study the analytical results in SDS93 therefore lend support to our numerical model.

Hereafter the growth rate of the eigensolutions, i.e. the imaginary part of the frequency  $\omega_i$ , will be denoted by  $\sigma$ . For each set of values of  $F, R, \beta$  we obtained the  $\omega_r - k$  curves or dispersion lines and the  $\sigma - k$  or instability curves for each mode,  $n$ . The instability curves show a span of unstable wavenumbers, namely  $\sigma(k) > 0$ , with a maximum  $\sigma$  for some  $k$  which will be denoted by  $k_M^n$  (fastest growing or dominant wavenumber corresponding to

mode  $n$ ), and whose growth rate will be  $\sigma_M^n$ . Typical instability and dispersion curves are shown in Figs 3–4. The dominant wavenumbers corresponding to the different modes are usually ordered as  $k_M^1 < k_M^2 < k_M^3 < \dots$ , that is, higher number modes have shorter dominant wavelengths. In contrast, the ordering of the maximum growth rates may change according to  $R$  for each given  $\beta$ . For small  $R$  we find  $\sigma_M^1 > \sigma_M^2 > \sigma_M^3 > \dots$  so that there exists a dominant mode (fastest growing mode) which is mode 1 (Fig. 3). In theory, this dominant mode and its wavelength could be compared to the topographic features observed in the field. On the other hand, Fig. 4 shows that for larger  $R$  we can have  $\sigma_M^1 < \sigma_M^2$  and even  $\sigma_M^1 < \sigma_M^2 < \sigma_M^3$ . The numerical procedure is, of course, not able to prove these inequalities for all mode numbers,  $n$ . In fact, in the latter case either the dominant mode would be a high mode or there would be no dominant mode, i.e. the  $\{\sigma_M^n, n = 1, 2, 3, \dots\}$  sequence could be unbounded. In general, the larger  $R$  is, the more complex the behaviour becomes. For instance, the instability curve for the first mode can have two relative maxima. Figure 5 shows that when  $R \sim 4$  the second maximum, which has a wavenumber comparable to the dominant wavenumbers for the higher modes, is the absolute maximum.

The curves showing  $\sigma_M$  or  $\lambda_M = 2\pi/k_M$  as a function of  $R$  for some  $F, \beta$  indicate the dominant instability mode and its wavelength for a given beach. As we can see in Figs 7 and 8, for small  $R$  the dominant mode is always mode 1, but for larger  $R$  higher modes can be dominant. In the former case a fairly periodic pattern with a low cross-shore complexity can be predicted. According to Figs 7 and 8 the corresponding alongshore wavelength is  $\lambda_M$

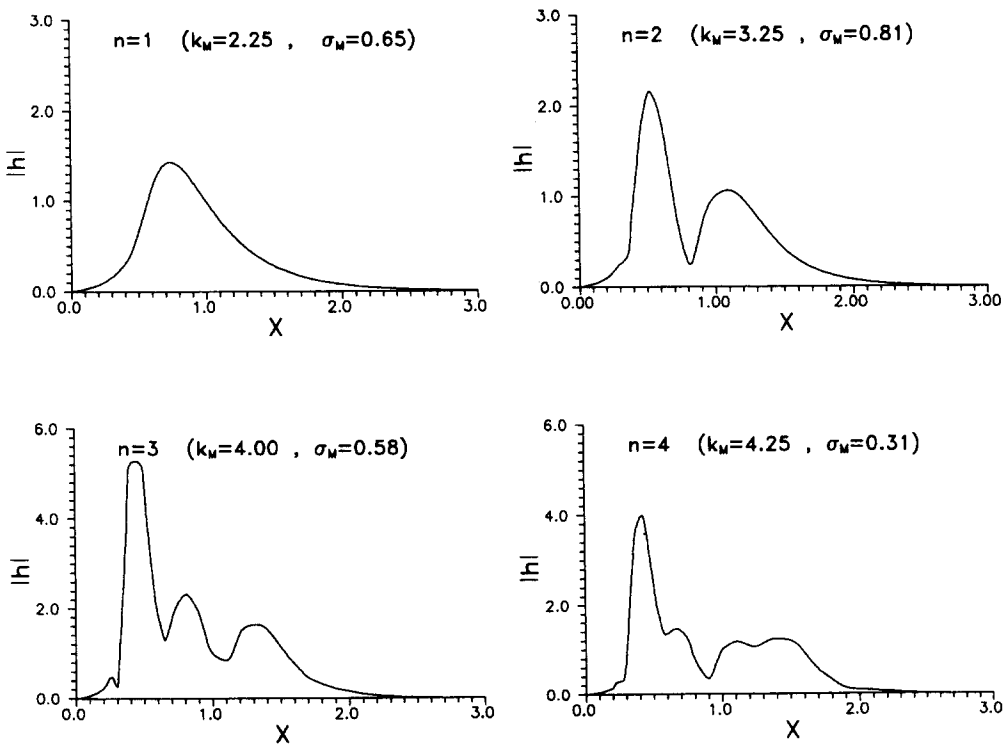


Fig. 2. Cross-shore structure of the perturbation of the sea bed for modes 1, 2, 3, 4. The modulus,  $|h(x)| = \sqrt{h_r(x)^2 + h_i(x)^2}$ , is shown,  $R = 1, F = 0.3, \beta = 0.01$ .

$\sim 4 - 8$ , that is, two to four times the surf zone width. We will refer to this case as the “low regime”. Different behaviour occurs for larger  $R$ , when mode 1 is no longer dominant. In this case a far more complex pattern appears in which shorter wavelengths can prevail ( $\lambda_M \sim 2$ ). We will refer to it as the “high regime”. The transition between both regimes is given by the intercept of the curves corresponding to modes 1 and 2 in the  $\sigma_M - R$  diagram. The critical values of  $F, R, \beta$  for this transition are presented in Fig. 6, where it can be seen that the transition moves to larger  $R$  for increasing beach slope,  $\beta$ .

Typically, the  $\sigma_M - R$  curve corresponding to each mode has a maximum, which indicates the beach parameters most conducive to the growth of this particular mode. The position of these maxima moves towards large  $R$  as  $n$  increases. In some cases the maximum instability occurs for mode 1 and for moderate values of  $R$ , say  $R \sim 0.5$  (see Fig. 7), whereas for other beaches the instability increases with  $R$  and with  $n$  outside the range of our numerical study (see Fig. 8). Typically, the former behaviour corresponds to steep beaches, say  $\beta \sim 0.02$  or more, and the latter one corresponds to gentle slopes, around  $\beta \sim 0.01$  or less.

For very small  $R$ , the growth rates,  $\sigma_M$ , are very small but positive, at least for mode 1. So, the  $\sigma_M - R$  curve for mode 1 seems to have a  $(0,0)$  intercept, and therefore there is no

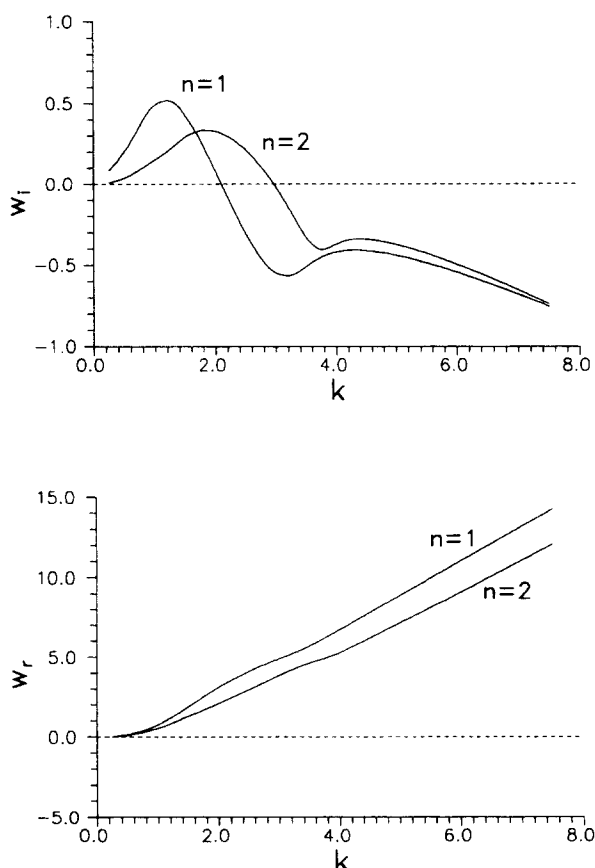


Fig. 3. Dispersion lines and growth rate of the instability, for  $R = 0.35, F = 0.3, \beta = 0.01$ .

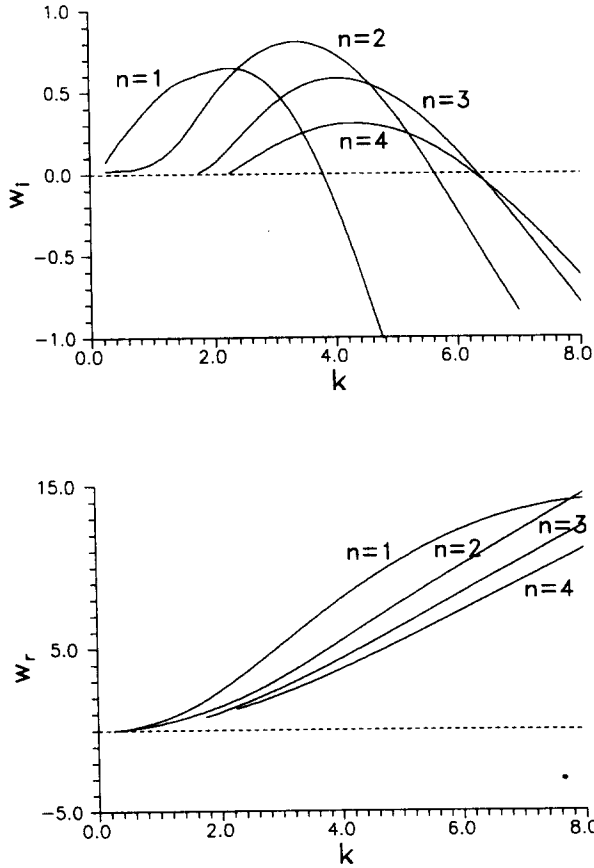


Fig. 4. Dispersion lines and growth rate of the instability, for  $R = 1, F = 0.3, \beta = 0.01$ .

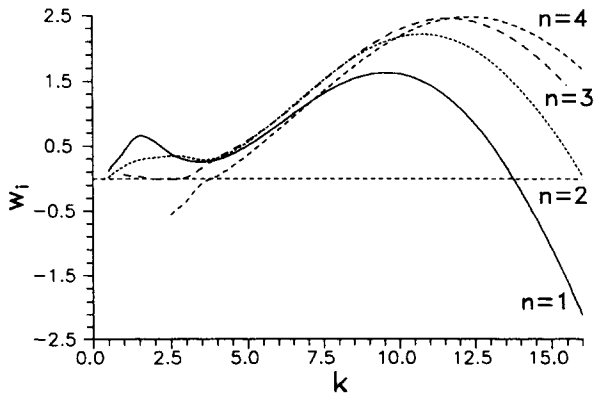


Fig. 5. Growth rate of the instability for  $R = 4, F = 0.1, \beta = 0.005$ . Note that mode 1 has two relative maxima and that the dominant one corresponds to a high wave number, in the range where mode 2 is dominant.

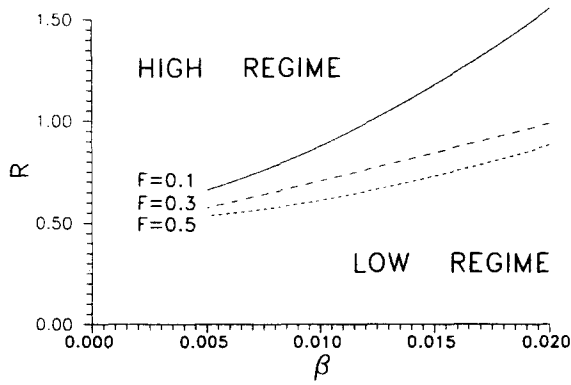


Fig. 6. Transition lines between “low” regime (mode 1 is the dominant mode) and “high” regime (other modes can be dominant) for several Froude numbers.

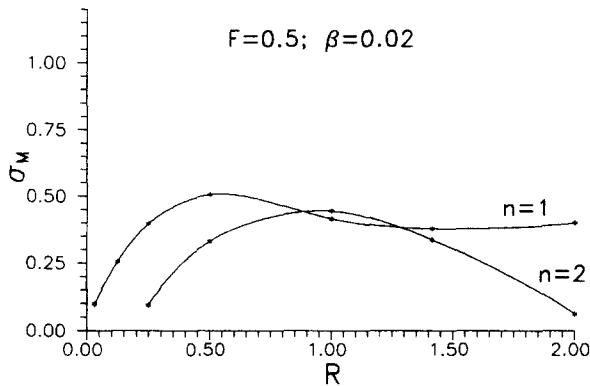
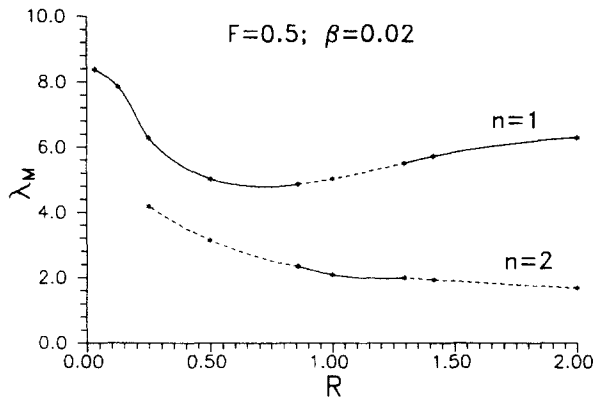


Fig. 7. Maximum growth rate of the instability and corresponding wavelength as a function of parameter  $R$ , for  $\beta = 0.02$ ,  $F = 0.5$ .

critical value  $R_c$  such that transition between stability and instability occurs. This has been seen by decreasing  $R$  either by decreasing  $c_d$  or by increasing  $\beta$ . Figures 7 and 8 also show how the dominant wavelength,  $\lambda_M$ , usually increases with decreasing  $R$ . Nevertheless, mode 1 may invert this behaviour around  $R \sim 1$  with a smooth increasing  $\lambda_M^1$  for  $R$  increasing above 1. For a very small  $R$  the dominant wavelength  $\lambda_M^1$ , is very large, with a very small growth rate.

The phase speed is always positive, making the sand waves migrate downflow. For a given set of parameters, the phase velocity depends on the mode and on the wavelength. For the fastest wavelength of the dominant mode,  $\lambda_M$ , the phase speed,  $c_r$ , is of the order of 1, increasing slightly from 0.8 to 1.3 as  $R$  increases. This can be seen, for example, in Fig. 3, where the fastest growing wavenumber of the dominant mode (1),  $k = 1.2$ , has  $c_r = 0.8$ . Figure 4 shows a corresponding phase speed of  $c_r = 1.1$  (mode 2,  $k = 3.2$ .) In addition, the typical growth time,  $\sigma^{-1}$ , can be compared with the period by means of the  $2\pi\sigma/\omega_r$  ratio. Figure 9 shows that for realistic values of  $R$  this ratio lies between 1 and 3, with a maximum near  $R \approx 0.5$ . This means that the sand waves can grow significantly in the time of taken to move one to one-third of wavelength.

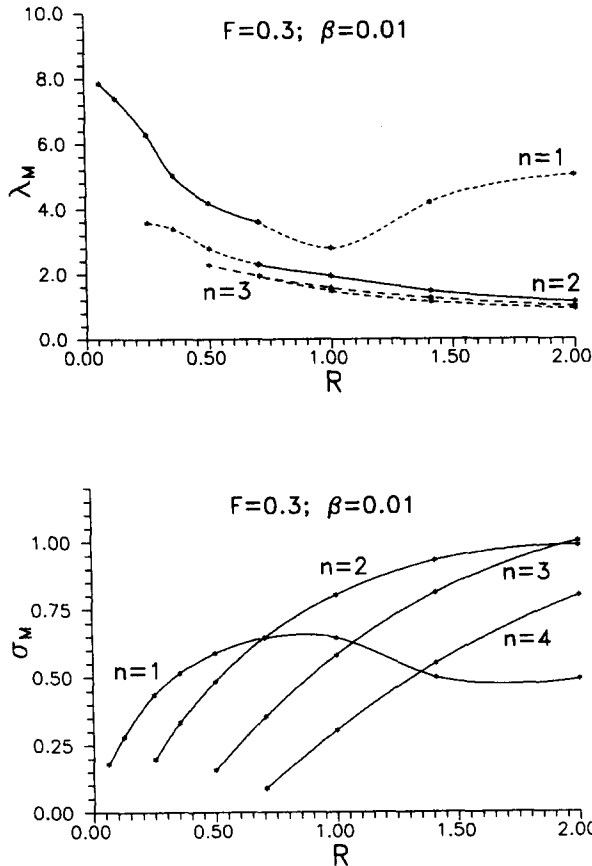


Fig. 8. Maximum growth rate of the instability and corresponding wavelength as a function of parameter  $R$ , for  $\beta = 0.01$ ,  $F = 0.3$ .

In Fig. 10 typical contour lines of the topographic perturbation corresponding to the first four modes are shown. The computation has been performed for  $R = 1$ ,  $F = 0.3$ ,  $\beta = 0.01$ . Mode 1 gives a simple transverse bars pattern. However, the higher modes display an oblique bar structure which has a downflow skewed shape similar to an “S”. Each wave crest has a series of secondary bumps and each wave trough a series of secondary holes.

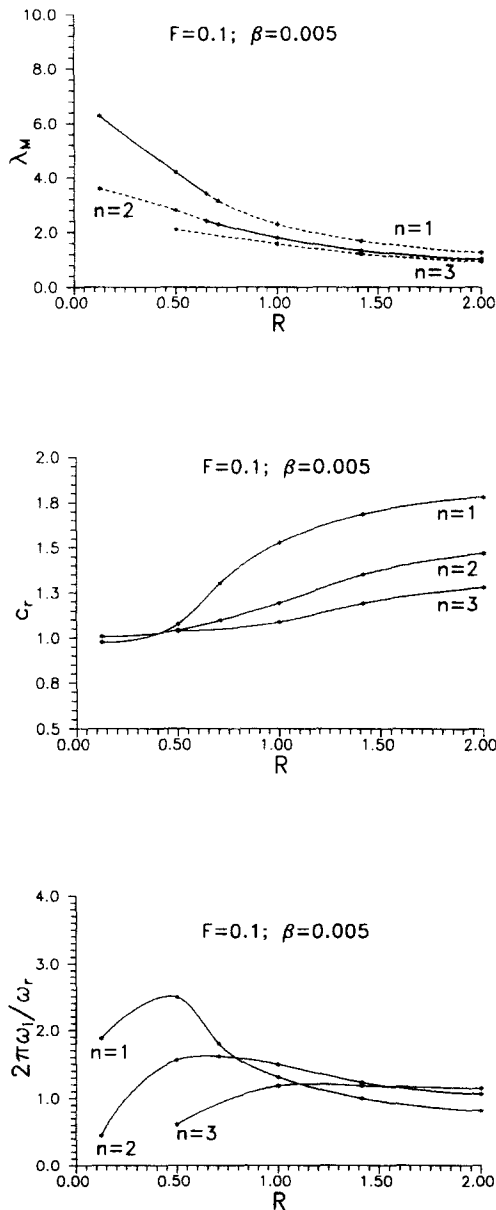
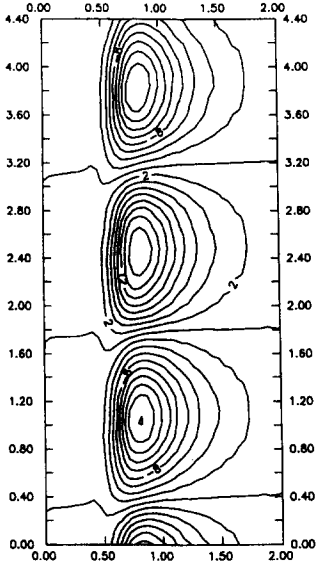
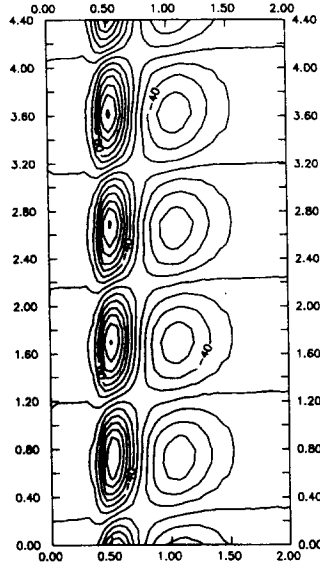


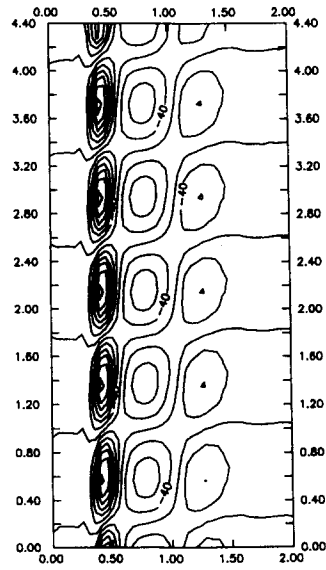
Fig. 9. Dominant wavelength,  $\lambda_M$ , phase speed,  $c_r$ , and ratio between the period and the typical growth time,  $2\pi\omega_i/\omega_r$ , as a function of  $R = c_d/\beta$ . Modes  $n = 1, 2, 3$  are shown.



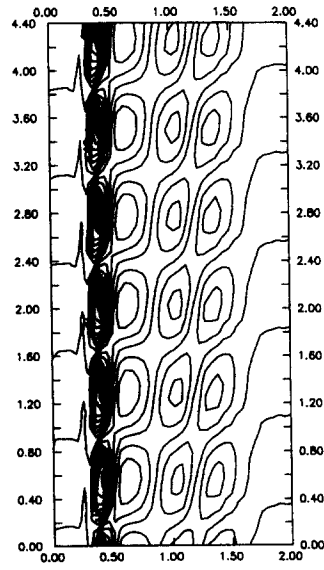
$n=1$  ( $k_M=2.25$ ,  $\sigma_M=0.65$ )



$n=2$  ( $k_M=3.25$ ,  $\sigma_M=0.81$ )



$n=3$  ( $k_M=4.00$ ,  $\sigma_M=0.58$ )



$n=4$  ( $k_M=4.25$ ,  $\sigma_M=0.31$ )

Fig. 10. Contour lines of the topographic perturbation for modes 1, 2, 3 and 4.  $R = 1$ ,  $\beta = 0.01$ ,  $F = 0.3$ ,  $k = 2.25$ .

The angles between the mean sand wave crest and the normal to the shore are approximately 3, 27, 40 and 58°. In Figs 11 and 12 the corresponding plots of the basic slope plus the perturbation are shown. The amplitude of the perturbation is not determined by the linear theory and has been chosen arbitrarily in order to obtain physically meaningful plots.

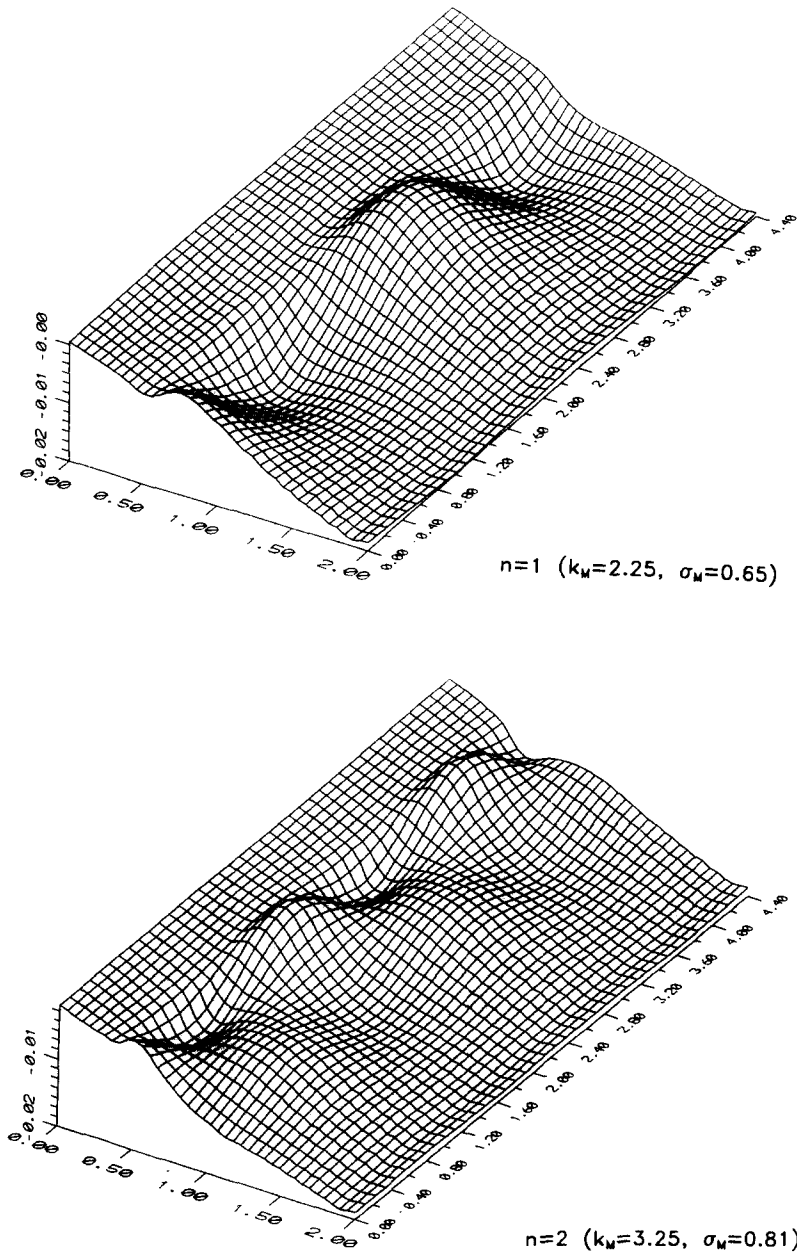


Fig. 11. Sand wave modes 1 and 2: basic slope + topographic disturbance. The amplitude of the disturbance has been arbitrarily chosen.  $R = 1$ ,  $\beta = 0.01$ ,  $F = 0.3$ ,  $k = 2.25$ .

These numerical results can be summarized as follows:

- (1) Within the explored range of parameters, which is the physically reasonable range of large-scale bedforms in the surf zone, instability has always been found. This instability leads to the initial growth of bedforms or sand waves propagating down-

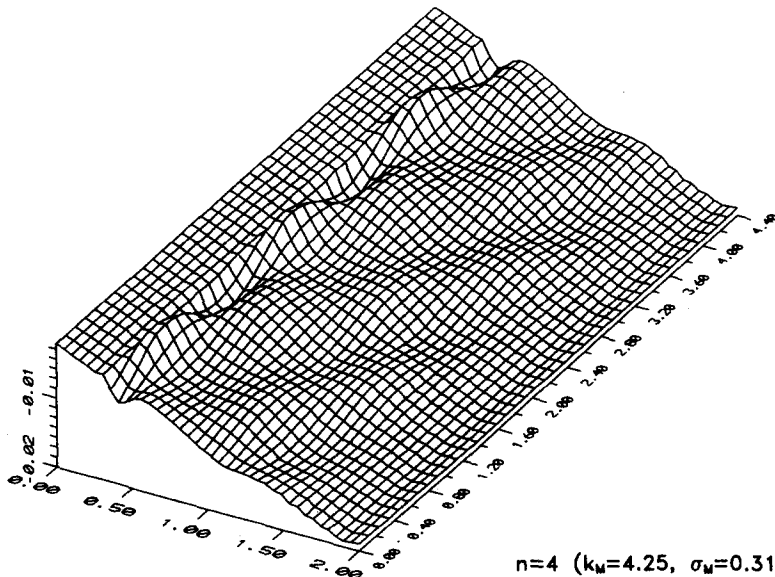
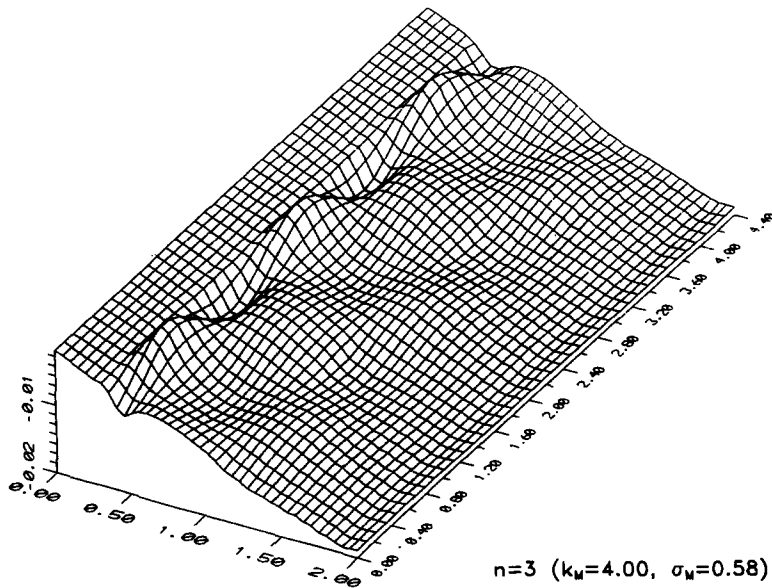


Fig. 12. Sand wave modes 3 and 4: basic slope + topographic disturbance. The amplitude of the disturbance has been arbitrarily chosen.  $R = 1$ ,  $\beta = 0.01$ ,  $F = 0.3$ ,  $k = 2.25$ .

flow. There are several sand waves modes numbered as 1, 2, 3 ... with increasing cross-shore complexity. Mode 1 is almost like a transverse bars system. The higher modes have a downflow skewed bathymetry with crests reminiscent of oblique bars. Secondary bumps and holes appear in their crests and their troughs.

- (2) The main parameter controlling instability was found to be  $R = c_d/\beta$ . Typically, for  $R \sim 0.1-0.7$ , increasing  $R$  gives rise to a monotonous increase in growth rates that for  $R$  up to 0.5 may be estimated by

$$\sigma_M \sim 0.9R^{0.6}. \quad (26)$$

A further increase leads either to a maximum growth rate and then to a smooth decrease or to a sustained increase depending on whether the slope is steep or gentle and also depending on  $F$ . For very small  $R$ , growth rates of modes 2, 3, ... are negative. However, the growth rate of mode 1 is very small but always positive. Therefore, transition does not exist, that is, there is no critical value,  $R_c$ , below which the basic flow is stable. Instead, for very small  $R$  the model gives very large beach features growing very slowly. This is clearly in contrast with the channel case (SDS93), and it means that for beaches with very small  $R$  there would always be large-scale unstable modes growing very slowly in time. From a physical point of view this is irrelevant due to the very small growth rates, but from a mathematical one it means that there is no transition and that a standard weakly nonlinear analysis would be impossible.

- (3) The wavelength of the fastest growing mode is usually a decreasing function of  $R$ , and typical values may be around two to eight times the distance from the shoreline to the peak longshore current. Assuming that this distance is about half the current width,  $X_b$ , the wavelength would be around one to four times  $X_b$ . The cross-shore location of the bedforms is similar to the location of the current.
- (4) The behaviour of steep beaches is simpler than the behaviour of gently sloping beaches. Any beach of the former type has a maximum unstable situation which corresponds to mode 1 for some  $R \sim 0.5$ . In contrast, bed-flow instability in very gently sloping beaches increases with  $R$  and  $n$ , apparently without bound (as far as we could see with the numerical model).
- (5) For every beach of slope  $\beta$ , if  $R$  is less than some critical value  $R_c(\beta, F)$ , the fastest growing mode or dominant mode is always mode 1. For larger values of  $R$ , higher modes may be dominant or there could even be no dominant mode. A natural beach which belongs to the first class would show a fairly periodic and simple pattern with transverse bars two to four times the width of the current apart. On the other hand, a beach of the second class would have a more complex downflow skewed bathymetry with bumps and holes in which shorter wavelengths could be dominant. In this latter case, even two different wavelengths can have the same growth rate yielding a quasi-periodic pattern. The critical value for this transition ranges from 0.5 to 1.3 and increases with increasing  $\beta$  and decreasing  $F$ . In general, it is found that the most complex sand wave pattern is exhibited by very gently sloping beaches with large bottom friction.
- (6) The dimensionless phase speed,  $c_r$ , is of the order of 1 (see Fig. 9) and the ratio between the period and the typical growth time ranges from 1 to 3 with the result that sand waves can grow significantly while they move only one-third to one wavelength.

## 4. THE PHYSICAL MECHANISM

The present section will be devoted to gaining insight into the physical mechanism underlying the model. A more thorough discussion including a comparison with other theoretical models and with experimental data will be presented in Section 5.

The behaviour of the sand waves (i.e. whether they grow or not, whether they migrate downflow or upflow, etc.) is governed by the phase lag between the periodic topographic pattern and the resulting periodic flow pattern. Growing bedforms need a convergence of sediment flux near the crests and divergence near the troughs. If such bedforms are downflow progressing, the maximum divergence of sediment transport (that is, the maximum erosion) should lag the wave crests in a phase  $\phi$ , such that  $\pi/2 < \phi < \pi$ . Therefore, given a disturbance on the bottom, we need to know the perturbation resulting in the flow. This problem was addressed in Falqués *et al.* (1993), but just some simple properties that can readily be seen from equations (16)–(18) are sufficient here for our purpose. We must emphasize that in contrast to Barcion and Lau (1973), this phase lag,  $\phi$ , is not assumed *a priori* but computed from the flow equations. For simplicity, we will assume  $V_c = 0$ .

Let us first assume that there is no bottom friction, that is,  $R = 0$ . Moreover, for simplicity, we will neglect downslope transport,  $\gamma = 0$ , which always produces a damping of instability [this can easily be seen from equation (29), where  $\gamma$  appears only in the diffusive terms]. Then, by substituting equation (22) in (18) we obtain

$$\left(\frac{\xi}{F^2 V^2} \eta_x\right)_x + \left(1 - \frac{\xi}{F^2 V^2}\right) k^2 \eta = k^2 h \quad (27)$$

[see Falqués *et al.* 1993, equation (5)]. Obviously, if we consider a real bottom disturbance,  $h$ , equation (27) implies that the free surface perturbation,  $\eta$ , will be real too, that is, will be in phase with respect to  $h$ . Then, according to equation (22),  $u$  will be imaginary, whereas  $v$  will be real. Finally, according to equation (20), the divergence of the sediment transport will be imaginary, that is, will have a phase lag of  $\phi = \pm\pi/2$  with respect to the bed wave crests. Therefore, in the absence of bottom friction the sand waves will be neutral waves, namely, waves propagating without growth. This is in line with SDS93 (p. 333). A few numerical tests that have been done for  $R = 0$  also lend support to this statement.

Let us now assume a one-dimensional flow. In this case, equation (16) requires no cross-shore variation in  $\eta$  and from the other equations no cross-shore gradients are allowed. So, assume also  $V_x = 0$ ,  $\zeta_x = 0$ . Then, a combination of equations (17) and (18) leads to

$$\nabla \cdot \vec{q} = \frac{\partial q_y}{\partial y} = imkV^{m-1}v = \frac{m\xi k^2 V^m}{3RF^2V^2 + ik\xi(F^2V^2 - \zeta^2)} h \quad (28)$$

so that the phase lag between divergence of sand transport and wave crests is given by  $\tan \phi = (\zeta^2 - F^2V^2)k\xi/3RF^2V^2$ , from where, if  $F < 1$ , we have  $0 < \phi < \pi/2$ . Therefore, in this case we find that there is no growth but a damping due to bottom friction (note that  $R = 0$  would again lead to  $\phi = \pi/2$ , i.e. neutral waves).

So far, similarly to the case of alternate bars in a channel, we have proved that bottom friction and two-dimensional flow are necessary conditions for growing bottom disturbances. For the channel case, instability needs a power in the transport formula larger than 1,  $m > 1$ . In contrast, some numerical tests indicated that this is not true for the coastal

case. The explanation for this is the following. From a combination of equations (18)–(20) we obtain

$$\frac{\partial h}{\partial t} + m \frac{V^{m-1}}{\xi} \frac{\partial h}{\partial y} - \beta \gamma \left[ \frac{\partial}{\partial x} \left( V^m \frac{\partial h}{\partial x} \right) + \frac{\partial}{\partial y} \left( V^m \frac{\partial h}{\partial y} \right) \right] = (m - 1) V^{m-1} \frac{\partial u}{\partial x} - \left[ m \frac{V d\xi}{\xi dx} + (1 - m) \frac{dV}{dx} \right] V^{m-2} u + m F^2 \frac{V^m}{\xi} \frac{\partial \eta}{\partial y} \quad (29)$$

in a close analogy with SDS93 [equation (3.18)]. Similarly to the channel case, the left hand side corresponds to an advection-diffusion equation that in the absence of forcing from the right hand side would describe decaying travelling sand wave solutions. The first term on the right hand side is similar to the single term in equation (3.18) of SDS93. However, the second one, related to the cross-shore gradients in the current and in the bathymetry, and the third one, related to the free surface, are new. If  $m = 1$ , the first term drops out but the second and third ones can produce unstable wave solutions, and they actually do, as we have found by numerical simulation.

The existence of a dominant wavenumber for each mode would be due to a balance between the forcing provided by the terms on the right hand side of equation (29) and the diffusive terms on the left. The latter terms are proportional to  $k^2$ , whereas the former ones are either proportional to  $k$  or not dependent on  $k$ . Therefore, short waves are stable. The behaviour of long waves is in contrast with the channel case as we found unstable waves with arbitrarily small wavenumbers. This can be understood as follows. When  $k \rightarrow 0$ , the diffusive terms in equation (29) and also the first and the third term on the right vanish. In contrast, the second term on the right, related to the cross-shore gradients in the basic state, does not vanish and therefore becomes dominant.

Finally, we will try to investigate why bottom friction yields sand wave growth and why this can only occur if cross-shore gradients are allowed. The explanation follows from a detailed examination of the potential vorticity. So, the first step is to derive a vorticity equation. This can readily be achieved by taking the curl of equation (2) and replacing  $\nabla \cdot V$  with its expression from equation (3) yielding:

$$\frac{d}{dt} \left( \frac{V_x + \Omega}{\xi} \right) = -c_d \frac{V \Omega}{\xi \xi} - c_d \frac{V}{\xi^3} \left( V \frac{\partial h}{\partial x} + \xi \frac{\partial v}{\partial x} \right) - 2c_d \frac{1}{\xi^2} \frac{d}{dx} \left( \frac{V}{\xi} \right) (Vh + \xi v) \quad (30)$$

where  $V_x = dV/dx$  is the background vorticity,  $\Omega = \partial_x v - \partial_y u$  is its perturbation, and  $(V_x + \Omega)/\xi$  is the total potential vorticity. Only linear terms have been kept on the right hand side and any perturbation of the forcing terms,  $\mathcal{F}$ , has been neglected. Then it is easily seen that if there is no bottom friction,  $c_d = 0$ , the potential vorticity is conserved. The first term on the right is a stabilizing one as it produces a decrease of disturbances on the background potential vorticity,  $V_x/\xi$ . However, the other two terms may produce a growth of disturbances if cross-shore gradients are allowed. So, bottom friction plays two roles in the vorticity dynamics: a damping one but also a (possibly) destabilizing one. Now we have to face the problem of finding the flow disturbance produced by a given bed perturbation. This problem has a simple analytical solution in the case where no cross-shore gradients in the basic state are allowed,  $V_x = 0, \xi_x = 0$  (channel flow, SDS93). Although some important physical effects can arise from these cross-shore gradients, especially from the background vorticity  $V_x$ , we believe that the physical mechanism of bed-flow instability is basically the same for both river and coastal environments. Therefore, we will focus on the

former one, which is mathematically much simpler. Also, since the surface effects are not essential, low Froude number,  $F \ll 1$ , will be assumed. For the sake of consistency, we will keep the notation of the coastal case. Thus, our  $(x, y)$  coordinates correspond to  $(-y, x)$  in SDS93 and our  $(u, v)$  to  $(-v', u')$ . Then, given a steady bed perturbation

$$h(x, y) = e^{iky} \cos px \quad (31)$$

flow equations (3.2) in SDS93 can readily be solved to find the resulting perturbation in the fluid motion:

$$u = \frac{kp(k - 3iR)}{D} e^{iky} \sin px, \quad v = \left(1 - \frac{p^2(3R + ik)}{D}\right) e^{iky} \cos px \quad (32)$$

where  $D = R(k^2 + 2p^2) + ik(k^2 + p^2)$ . In  $R = c_d/\beta$ ,  $\beta$  has been defined as the depth to width ratio. If bottom friction is neglected, it can be seen from these equations that the maximum longitudinal velocity,  $V + v$ , occurs over the bar crests,  $y = 0$ , and the minimum on the troughs,  $y = \pi/k$ , so that neutral sand waves travelling downcurrent result. Moreover, the streamlines follow the topographic contours without lag [see Fig. 13(a)] and, according to equation (30), there is no vorticity,  $\Omega = 0$ . Over the crests,  $v$  decreases by moving away from the channel bank, that is, increasing  $x$ , and this decrease achieves its alongshore maximum at the crests. Therefore,  $\partial v/\partial x$  is negative and has its minimum there. Then, in the absence of vorticity,

$$\frac{\partial u}{\partial y} = \frac{\partial v}{\partial x} - \Omega \quad (33)$$

implies that also  $\partial u/\partial y$  will have its minimum at the crests. Notice that this alongshore minimum coincides with the location where the streamlines turn inshore,  $u = 0$ , because  $u$  depends harmonically on  $y$ . These statements can be derived from equation (32).

When bottom friction is taken into account, equation (32) shows that the maximum longitudinal velocity lags the bed crests, so that the phase lag between divergence of sediment transport and bed crests becomes  $\phi > \pi/2$  and, therefore, the bars grow. The occurrence of this phase lag can be understood in terms of the vorticity. Let us first consider the case of an isolated transverse bar. Consider a fluid particle initially without vorticity and approaching the bar, convected by the undisturbed flow velocity,  $V$ . As soon as the particle approaches the bar, it will find a transverse slope  $\partial h/\partial x < 0$  and thereby also a gradient  $\partial v/\partial x < 0$  because flow tends to go faster in shallow rather than in deep water due to mass conservation. Then, looking at vorticity equation (30), we find that the second term on the right will be positive and will therefore create vorticity. The rise in vorticity will continue until a balance involving the first term is achieved. This process can easily be understood in terms of the torque due to the excess of frictional forces per mass unit in shallower water, both depth being smaller and the current stronger. Now let us assume an alongshore periodic sand wave train and a small bottom friction,  $c_d$ . In that case, the vorticity will be also alongshore periodic. Taking into account again the sign of  $\partial h/\partial x$  and  $\partial v/\partial x$ , according to equation (30), the vorticity of a fluid particle will tend to increase over the crests and decrease over the troughs. Therefore, its maximum will be somewhere slightly downstream of the crests. Looking again at equation (33), we see that the location where the streamlines turn inshore, that is, where  $\partial u/\partial y$  achieves its minimum, will now be slightly shifted downstream. Then, as shown in Fig. 13(b), the streamlines will diverge at the crests and owing to  $F \ll 1$ , by mass conservation, this will produce a maximum

longitudinal velocity slightly upstream of the crests rather than over the crests. As we have seen, this produces the growth of the bars.

### 5. DISCUSSION

Dimensional magnitudes will be used throughout this section, and the subindex  $M$  in  $\lambda_M$ ,  $\sigma_M$  will be dropped out for the sake of simplicity, so that  $\lambda$ ,  $\sigma$  refer to the dimensional

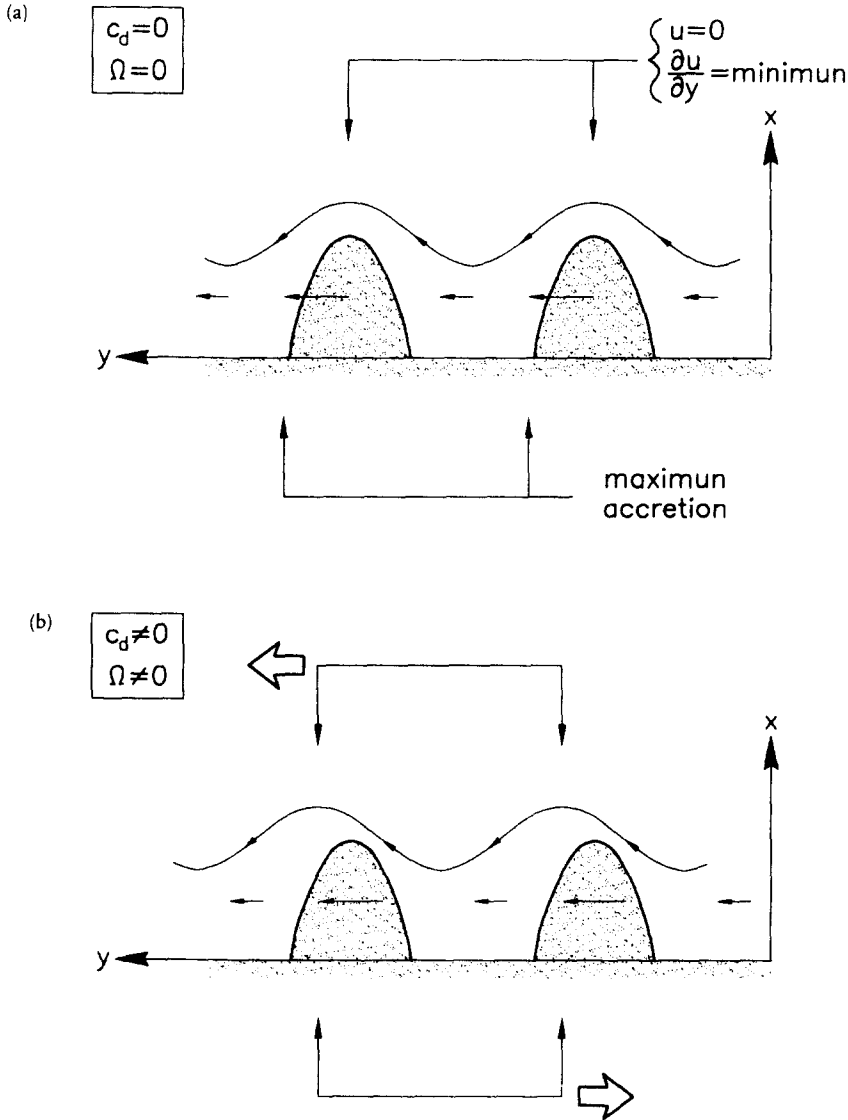


Fig. 13. Sketch of the perturbation in the current caused by a sand wave train without bottom friction (a), and with bottom friction (b). A typical streamline and the location of the maximum and minimum longshore component are shown. The shifts produced by bottom friction are indicated in (b).

dominant spacing and growth rate of the topographic waves. Any application of bed-flow instability mechanism to field conditions will essentially have to do with topographic features that: (1) display some alongshore periodicity, and (2) migrate downcoast, along with a correlated meandering in the longshore current with, possibly, a correlated rip currents system. Alongshore rhythmic topographic patterns with horizontal lengthscale of the order of the surf zone width are commonly known as rhythmic topography (Sonu, 1973; Wright and Short, 1984; Lippmann and Holman, 1990). Rhythmic topography is revealed very often by a system of sand ridges which joint the shoreline and are known as transverse or oblique bars, depending on whether they are normal to the coast or skewed. They were called cusp-type sand waves by Sonu (1969) and defined as a series of crests and troughs along the shore. Each crest starts in a cusp on the shoreline and extends offshore. Transverse/oblique sand bar systems have been reported by many authors from open coasts (Evans, 1939; Hunter *et al.*, 1979; Chappell and Eliot, 1979) or from sheltered beaches (Niedoroda and Tanner, 1970; Barcilon and Lau, 1973; Falqués, 1989). Abundant sand supply and very gentle slopes are conditions favouring their formation, and Evans (1938) pointed out that they are characteristic of beach profiles above equilibrium profile. Figures 14 and 15 provide two examples of oblique bar systems on high and on low energy beaches.

Even though the morphological instability mechanism based on the longshore current was probably the first invoked to explain rhythmic beach topography (Sonu, 1969), little attention has been paid to it in comparison with mechanisms based on edge wave activity. Bowen and Inman (1971) showed how the net drift velocities associated with an infragravity standing edge wave (periods of 30-60 s) could provide an explanation for crescentic bar formation. Although this mechanism seems well suited to crescentic bars between headlands its extension to long straight beaches is not obvious, especially for wave lateral incidence where progressive edge waves rather than standing ones are expected. Holman and Bowen (1982) relaxed the hypothesis of standing edge waves and looked at any interaction of two progressive edge modes of the same frequency but different mode number and wavelength. They found that some combinations of edge waves lead to topographic patterns highly reminiscent of observed rhythmic features like, for instance, oblique bars. However, the theory lies on the hypothesis of phase-locked interacting edge waves and it is not obvious why edge waves excited in natural beaches should be coherent and whether they actually are or not (Huntley, 1988). Several field studies provide evidence for the interaction between infragravity edge waves and rhythmic topography. Wright *et al.* (1986) and Aagaard (1991) obtained infragravity wave energy peaks at periods corresponding to edge waves of wavelengths highly correlated to the existing rhythmic topography at that moment. In a more detailed study, Bauer and Greenwood (1990) proved the presence of a mode 3 standing edge wave and showed how an initial linear longshore bar tended towards a crescentic bar in response to the forcing by this wave. In spite of all these efforts, Aagaard stated: "the definitive verification of the validity of the infragravity model has not yet been accomplished". Even though there is no doubt that crescentic bars and infragravity edge waves do often exist together, there are some cases where these waves are controlled by the inherited topography rather than being forced by the grouping of incident waves (Wright *et al.*, 1986). This suggests that even if topography-linked edge waves are present, it might happen in some cases that they are not the initial driving mechanism.

For lateral wave incidence, even if edge waves are present, the morphological role of the

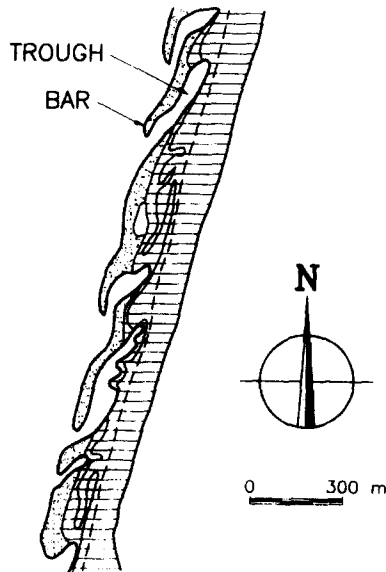
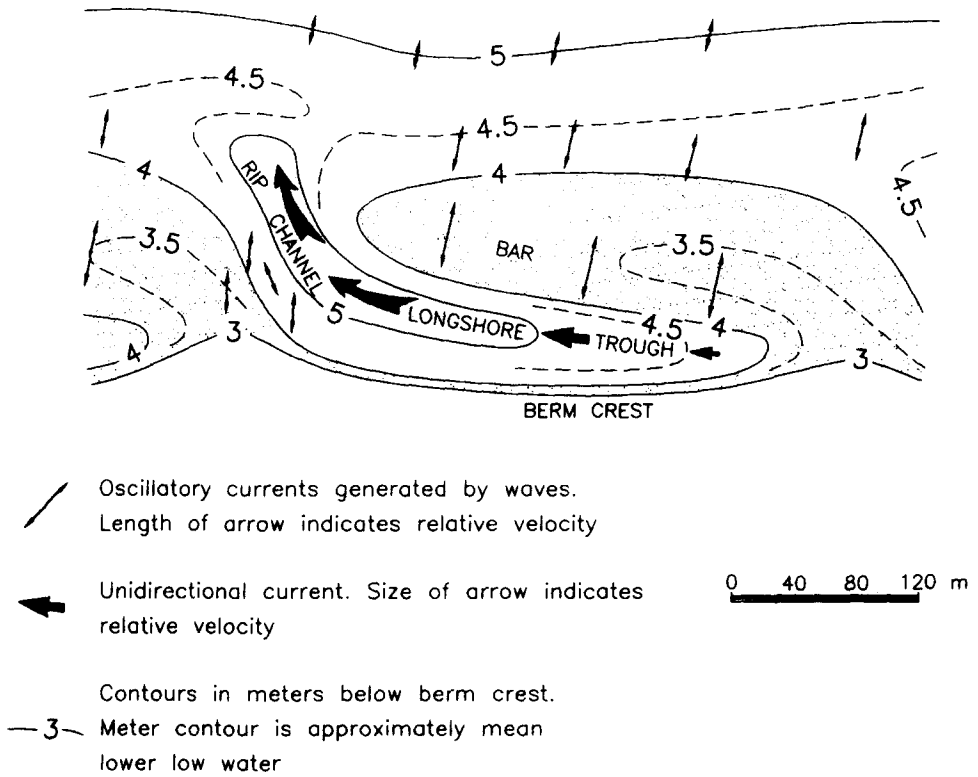


Fig. 14. Welded oblique bars on an open coast (Oregon, U.S.A.) after Hunter *et al.* (1979).

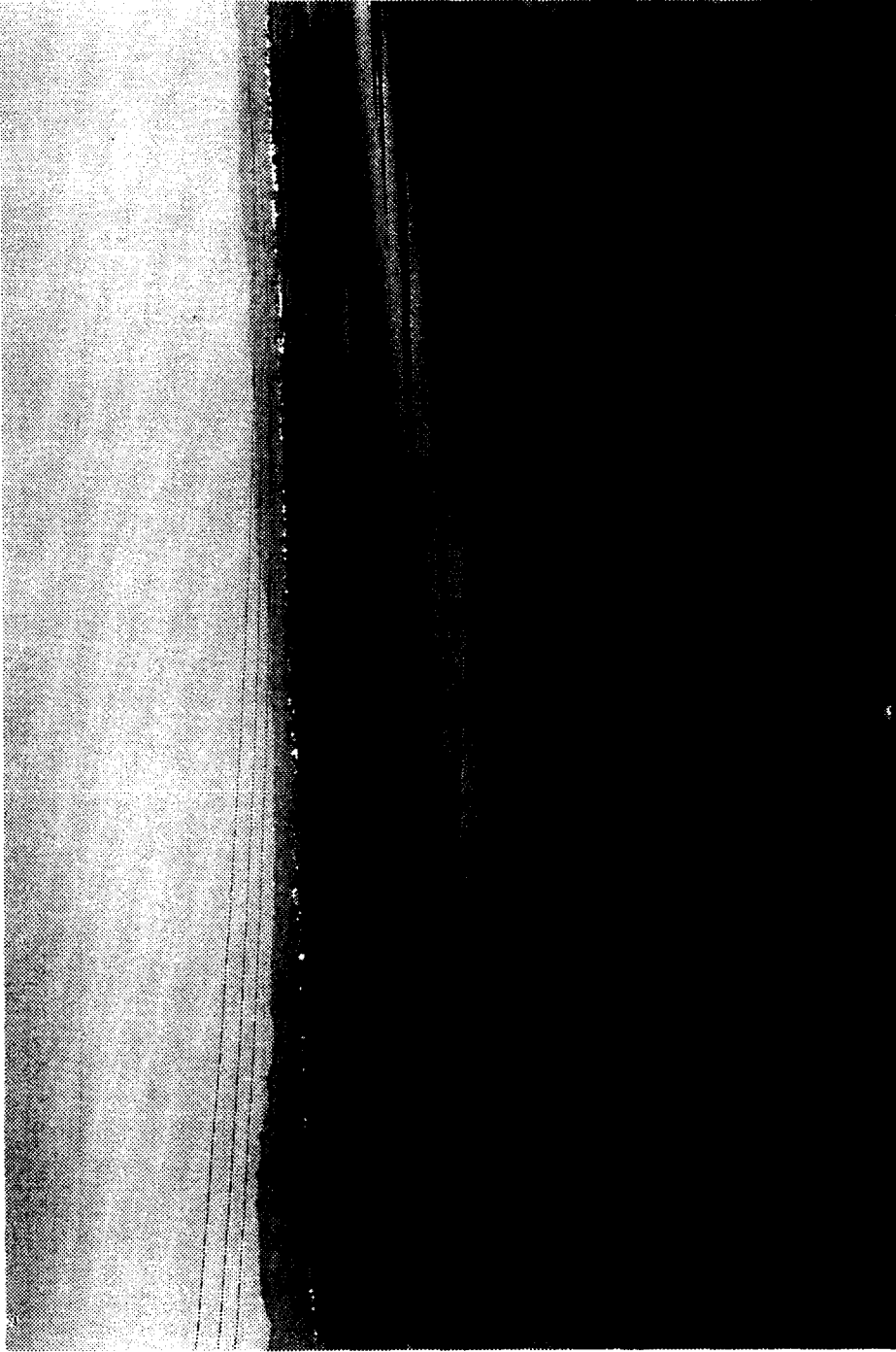


Fig. 15. Transverse/oblique bars in a low energy beach. Trabucador Beach, Alfacs Bay (Ebro Delta, Spain). Mean spacing,  $\lambda \sim 20$  m and bottom slope,  $\beta \sim 0.01$ .



longshore current should not be underestimated, as it seems to have been for a long time. In a first instance, the longshore current can significantly disturb the edge wave characteristics (Falqués and Iranzo, 1992). But of major importance is that longshore currents can easily reach values of up to  $1\text{--}1.5\text{ m s}^{-1}$  and have therefore an obvious capability for sediment transport and thereby morphological activity. Evidence for this activity at lengthscales relevant to surf zone dynamics is well established from alternate bar formation in river environments (SDS93). Therefore, it seems conceivable that the same physical mechanism as in rivers could operate in the surf zone environment even if other physical processes like edge wave activity or bed-surf instability also occur. Thereby, the predictions of the present model should apply to the initial stage of growing rhythmic features wherever there is a significant longshore current. We have nevertheless to keep in mind that the results of the model depend on the cross-shore extension and distribution of the longshore current. Therefore, the appropriate environmental conditions would be the surf zone of any sandy beach under lateral wave incidence. From equation (26) the dimensional growth rate can be easily obtained. First and according to the scaling defined in Section 2, the morphological timescale is  $T = \beta L^2/Q$ , where  $Q = \nu U^m$  is of the order of the peak sediment transport,  $\nu(U - V_c)^m$ , and can be considered as a characteristic rate of sediment transport (volume per width unit and time unit). Then, taking into account  $L = 0.5X_b$  and  $\lambda \sim 3X_b$  we obtain a dimensional growth rate

$$\sigma \sim 32 \frac{c_d^{0.6} Q}{\beta^{1.6} \lambda^2}. \quad (34)$$

Therefore, the typical growth time  $\sigma^{-1}$  is longest for the largest features. Typical values of the sand transport rate  $Q$  for current intensity of order  $1\text{ m s}^{-1}$  may be of the order of  $10^{-4}\text{ m}^2\text{ s}^{-1}$  (Osborne and Vincent, 1993; Horikawa, 1988) so that for  $c_d \sim 0.005$  and  $\beta \sim 0.01$  growth times of the order of 13 h are obtained for rhythmic topographies with a spacing of 100 m and of the order of 5 days for a spacing of 300 m. These orders of magnitude are in agreement with that observed, for instance, by Lipmann and Holman (1990): "Initial formation of longshore variability may be quite rapid, commonly less than 1 day after the peak of high wave events. Continued periods of low wave energy generally result in the formation of large scale three-dimensionality, with time scales of 5–7 days." A rough dependence of the dimensional growth rate on the height of the incoming waves,  $H_b$ , can be obtained from the Longuet-Higgins model (Horikawa, 1988), which gives a longshore current scale  $U \sim (\sqrt{\gamma_b g H_b}/R) \sin \alpha_b$  where  $\gamma_b \sim 0.8$ , and where  $\alpha_b$  is the angle of wave incidence. A combination of this expression with the definition  $Q = \nu U^m$  and equation (34) gives:

$$\sigma \sim 3.6 \nu g^{m/2} \gamma_b^{(m+5)/2} \frac{c_d}{R^m} H_b^{(m-4)/2} (\sin \alpha_b)^m \quad (35)$$

where it is seen that growth rates increase with the incidence angle, in agreement with Sonu's statement that lateral wave incidence favours rhythmic topography development. If the power  $m$  in the transport formula is smaller than 4, the growth rate in equation (35) increases with decreasing wave energy (a very common value is  $m = 3$ , and we took 2 in the numerical model). This might seem senseless because waves are the energy input, but it is easily understood assuming some ratio  $r = \lambda/X_b \sim 4$  and a relationship between wave height and local depth at breaking  $\gamma_b = H_b/\zeta_b$ . Then, it appears that

$$\lambda = \frac{r}{\gamma_b \beta} H_b \quad (36)$$

from where the geometrical control in equation (34),  $\lambda^2$ , increases faster than the sediment transport,  $Q$ , under rising wave height (for  $m < 4$ ). This is in agreement with the experimental observation that rhythmic features are most often seen under moderate and falling wave energy. Note that equation (35) would predict an increasing growth rate without bound for very small wave amplitude, which, of course, is unrealistic. This is due to the fact that the present model calculations are for only one value of the threshold velocity for sand transport,  $V_c = 0.05U$ . In fact, some calculations done with  $V_c = 0.1U$ ,  $0.5U$ ,  $0.8U$  show that for  $V_c \sim U$  the non-dimensional growth rate decreases for increasing  $V_c/U$  so that the trend is reversed and as a result, the dimensional growth rate also decreases to zero for lowering wave energy.

Sonu (1969) noted that the migrational speed of sand waves,  $V_{mi}$ , decreases with increasing wavelength, being proportional to  $\lambda^{-4/5}$ . In view of the inherent large error bars,  $V_{mi}$  was proposed to be roughly proportional to  $\lambda^{-1}$ . The dimensional phase speed is  $V_{mi} = c_r L/T$ , where  $T$  is the morphological timescale and  $L = 0.5X_b$  the lengthscale. Taking into account that from the model calculations the dominant wavelength is  $\lambda \sim 3X_b$ , and that the non-dimensional phase speed,  $c_r$ , is of the order 1, the migration velocity for the dominant mode would then be

$$V_{mi} \sim 6 \frac{Q}{\beta \lambda} \quad (37)$$

in concordance with Sonu's statement. Clearly, as Sonu also suggested, the migrational speed also depends on the strength of the current in such a way that any prediction based on the field data presented in his article (Fig. 11) should be handled with care as there is no information on the currents. However, assuming the  $\lambda^{-1}$  dependence, one can infer from the smaller sand waves in Sonu's Fig. 11:  $V_{mi} \sim 1.4 \times 10^3/\lambda$  (in  $\text{m day}^{-1}$ ,  $\lambda$  in  $\text{m}$ ). This estimate, assuming  $\beta \sim 0.01$ , is in agreement with Sonu's equation (3.2) for a sediment transport of  $Q \sim 3.0 \times 10^{-5} \text{ m}^2 \text{ s}^{-1}$  which is not unrealistic at all. An application of equation (3.2) to the laboratory experiment reported by Sonu (1973), with  $\beta = 0.05$ ,  $\lambda \approx 3 \text{ m}$ ,  $U \sim 0.3 \text{ m s}^{-1}$  and  $V_{mi} \approx 1.1 \times 10^{-4} \text{ m s}^{-1}$  would give  $Q \approx 2.8 \times 10^{-6} \text{ m}^2 \text{ s}^{-1}$  which also seems realistic taking into account that the current was two or three times smaller than typical values for field conditions. By introducing this value of  $Q$  into equation (34) we obtain a growth time of 4 h, which is in rough agreement with the experimental results.

Another important issue of morphodynamic models of rhythmic topography is the alongshore spacing or wavelength,  $\lambda$ . Although that reference to rhythmic topography is very common in the literature, data on spacing along with mean bottom slope and surf zone width is not so common. An indirect data source comes from the spacing between rip currents, which are assumed to be linked to rhythmic topography. Then, the many existing field observations of rip currents (see, for instance, Sasaki and Horikawa, 1975; Huntley and Short, 1992) lead to an observed wavelength to surf zone width mean ratio around  $\lambda/X_b \sim 3 - 4$ , but with a scatter from 1.5 to 8. The available direct observations of topographic features correspond, indeed, to this ratio. For instance, field data from Oregon reported by Hunter *et al.* (1979) gave a ratio of 6. The authors observed ratios between 1.5 and 4.5 in Trabucador Beach, a low energy beach in the Ebro Delta (see Fig. 15). In the experiment reported by Sonu (1973) a 1.9 ratio was observed. All this is not in

disagreement with the present model, which gives a ratio ranging from 1 to 4. For values of  $R$  up to 0.3, which are very common, the dominant mode is mode 1 and the corresponding ratio then ranges between 3 and 4.

As was mentioned in Section 1, Hino (1975) considered the full instability of a beach under wave attack, incorporating both instability mechanisms, bed-surf and bed-flow. For lateral wave incidence, namely, when the bed-flow mechanism is in operation, some comparison between his analysis and the present one can be made. Even with regard to the bed-flow mechanism, there are many differences between Hino's model and the present one. His current profile is linear up to the breaker line and then falls to zero. The bottom friction and the sand transport are both linear in the velocity ( $m = 1$ ). The numerical model has some similarity with ours in that it is based on a Galerkin expansion, but the resolution is very low ( $N = 8$ ) and at the end a more severe truncation is made. In spite of these differences a  $\lambda/X_b \approx 4$  ratio is obtained, very similar to that given by the present model. Unfortunately, Hino's paper does not give many details and no distinction is made in this final result between normal and lateral wave incidence. One has to assume that the ratio of 4 is not likely to depend on the angle. This would not be surprising if we assume that bed-surf alone (normal incidence) gives a ratio of 4 and we take into account that bed-flow mechanism gives a ratio of 3–4. More recent research by Christensen *et al.* (1995) has reproduced Hino's analysis and no preferred wavelength was found. This discrepancy may perhaps be due to their assuming that the incoming waves were Rayleigh distributed instead of regular as Hino did. Another possibility is the low numerical resolution of Hino's numerical model. In the case of more realistic sediment transport modelling (either similar to ours with  $m = 3$  or suspended load) a wavelength  $\lambda \approx 6X_b$  is obtained. Apparently, no instability is found for normal incidence. This would mean that bed-flow instability should be the prevailing mechanism rather than bed-surf. Clearly, it appears that there is a need for more extensive research with a unified numerical model with the capability to select either of the two instability mechanisms or both together, to choose between several sediment transport models and to use alternatively regular or irregular waves. In addition to morphological instability models like the present one or Hino's model, purely hydrodynamic models can also account for the correct rip current spacing. For normal wave incidence, Miller and Barcilon (1978) found that the basic steady solution lacked uniqueness so that there can be a steady equilibrium with horizontal circulation cells. Curiously, the spacing between these eddies,  $\lambda$ , has also values between 1.5 and 8, and is a decreasing function of the parameter  $R = c_d/\beta$ .

Barcilon and Lau (1973) reported some field observations on transverse bar systems in low energy beaches. Some other data on sheltered beaches are also available from Niedoroda and Tanner (1970), Sonu (1973) and Falqués (1989) (see Table 1). It is revealed that the spacing increases with decreasing bottom slope, so that the parameter  $\beta\lambda$  does not vary very much, keeping values between 0.15 and 1 while the spacing,  $\lambda$ , ranges from 3 m (laboratory experiment; Sonu, 1973) to 1000 m (see Fig. 16). If edge waves were responsible for the rhythmic spacing, since the wavelength,  $\lambda_{ew}$ , of an  $n$  mode edge wave of period  $T_{ew}$  is given by

$$\lambda_{ew} = \frac{1 + 2n}{2\pi} g T_{ew}^2 \beta \quad (38)$$

it would be expected that rhythmic topography spacing increases with beach slope. This should happen if the period and the mode number were more or less fixed by the forcing,

but just the opposite trend is seen from the low energy data set out in Table 1. For the moderate to high energy beach data collected,  $\beta\lambda$  ranges between 1.4 and 6. In this case, the tendency of the spacing to increase with decreasing beach slope is not so clear, but at least, there is no tendency to decrease. This trend of  $\lambda$  to not increase with the beach slope,  $\beta$ , is not surprising because, owing to equation (36), the parameter  $\beta\lambda$  depends on the breaker amplitude through  $\beta\lambda = rH_b/\gamma_b$ . This suggests that the cases reported by Barcilon and Lau could be related to bed-flow instability for wave driven currents (rather than tidal or river-discharge) or to bed-surf instability (especially wave refraction, see Niedoroda and Tanner, 1970). In the case of edge wave related features, the tendency of

Table 1. Mean beach slope and spacing corresponding to observed rhythmic topography

Mean beach slope $\beta$	Mean alongshore spacing $\lambda$ (m)	Low/high energy	Site*
0.00082	640	L	5
0.001	1000	L	4
0.0015	218	L	3
0.0015	140	L	6
0.0035	50	L	7
0.0045	64	L	2
0.0066	23	L	8
0.01	60	L	1
0.01	20	L	1
0.05	3	L	9
0.005	370	H	12
0.01	600	H	10
0.01	500	H	14
0.01	136	H	11
0.017	75	H	15
0.02	300	H	16
0.02	250	H	13
0.03	92	H	17

\*Numbers correspond with the following beaches:

- 1 Trabucador Beach, Ebro Delta, Spain.
- 2 Florida, U.S.A. (Niedoroda and Tanner, 1970).
- 3 Florida, U.S.A. (Niedoroda and Tanner, 1970).
- 4 Mansel Island, Canada (Barcilon and Lau, 1973).
- 5 Bethany Beach, Delaware, U.S.A. (Barcilon and Lau, 1973).
- 6 St James Island, Florida, U.S.A. (Barcilon and Lau, 1973).
- 7 Ochlockonee Point, Florida, U.S.A. (Barcilon and Lau, 1973).
- 8 Silver Lake, Michigan, U.S.A. (Barcilon and Lau, 1973).
- 9 Laboratory experiment by Horikawa and Sasaki (Sonu, 1973).
- 10 Crescentic bar, Australia (Wright *et al.*, 1978).
- 11 Crescentic bar + transverse bars, Australia (Wright *et al.*, 1978).
- 12 Welded oblique bars, Australia (Chappell and Eliot, 1979).
- 13 Crescentic bar, Australia (Wright *et al.*, 1986).
- 14 Mean values crescentic inner bar, central Dutch coast (Short, 1992).
- 15 Georgian Bay, Canada (Bauer and Greenwood, 1990).
- 16 Oregon, U.S.A. (Hunter *et al.*, 1979).
- 17 Lake Michigan, U.S.A. (Evans, 1939).

the spacing not to increase with increasing beach slope suggests that infragravity edge waves would very often be controlled by the topography rather than the period of the grouping of the incident waves, and therefore in accordance with the observations by Wright *et al.* (1986) and also with Huntley and Short (1992).

For  $R$  up to 0.5, which is very common in natural beaches, "low regime" prevails in the model, yielding transverse bars with a slight downcurrent skewness. This is not inconsistent with the observed transverse bars in low energy beaches but does not compare well with the welded bars on open coasts, which are very often almost parallel to the coast. The higher modes of the present model, which may be rotated  $60^\circ$  in the downcurrent direction, would be more suited to the latter case. This would nevertheless require  $R$  higher than 0.5, which is not very realistic except for, maybe, a rippled bed and/or beach profile well above equilibrium. Models that incorporate the bed-surf in addition to the bed-flow mechanism predict oblique bars for lateral wave incidence. However, Hino (1975) predicts downcurrent rotated crests whereas Christensen *et al.* (1995) predict upcurrent rotated crests. According to Christensen *et al.* (1995), this discrepancy might be explained by the differences in the longshore current profiles. But the point is that all the available observation of surf zone welded or oblique bars report downcurrent or down-wave skewness. It should be borne in mind, however, that all these models describe only the initial development of topographic features since they are based on linearized equations for small amplitude perturbations. When the bars grow significantly all the different mechanisms strongly interact and even though one mechanism may have been the driving one at the initial stage another can become dominant, imposing its own characteristic pattern. For instance, even if bed-flow was dominant at the initial stage, as soon as bedforms develop according to the present model, the incoming waves would be

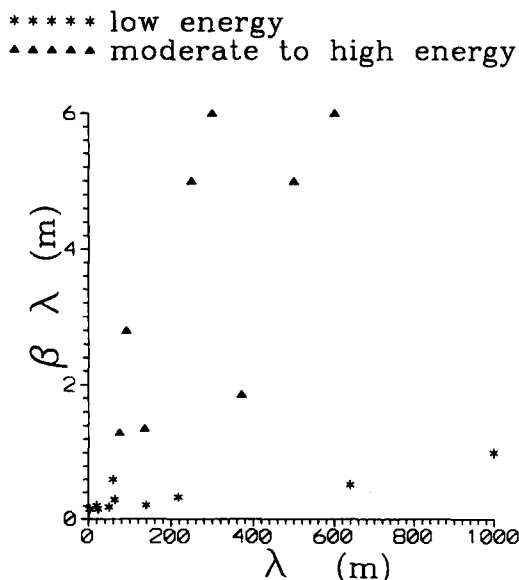


Fig. 16. Beach slope,  $\beta$ , and mean spacing,  $\lambda$ , for rhythmic topography on several beaches ranging from low to high energy.

disturbed and bed-surf mechanism would start to operate, modifying the initial shape of the bedforms.

The model based on edge waves (Holman and Bowen, 1982) yields topographic patterns most reminiscent of observed welded bars on open coasts (see, for instance, Fig. 6 in their paper). This might be due to the fact that, although small amplitude edge waves are used, an equilibrium solution rather than an initial development is obtained. This concordance and the observation of edge waves linked to rhythmic topography prove that infragravity edge waves are, indeed, a very important factor for the development and maintenance of such topographic features but do not imply that they will always be the initial driving mechanism.

In addition to river and surf zone sand bars, the bed-flow instability mechanism could also explain larger scale coastal topographic features like offshore generated sand waves eventually reaching the shoreline [as observed in the Nile Delta by Inman *et al.* (1993)]. It could also have some influence on shore connected sand ridges in the shelf [as observed on the Dutch coast; Van de Meene (1994)]. Our numerical model can therefore be applied to these sedimentary patterns. However, the validity of the present available results is restricted to the surf zone, as they drastically depend on the longshore current width and distribution.

## 6. CONCLUSIONS

It has been found that the longshore current on an erodible beach can be unstable due to the positive feedback between topographic disturbances and flow disturbances. The instability occurs as a result of the vertical vorticity generated by the topographically induced differences in bottom friction. Therefore, even though the mechanism is conceptually similar to the dune or antidune growth mechanism for one-dimensional channel flow hypothesized by Sonu (1969) as an explanation for rhythmic topography, its two-dimensional geometrical nature makes it essentially different. Thus, the closest analogy may be found in the occurrence of alternate bars in a river. The instability causes the growth of alongshore periodic beach topography, downflow progressing or sand waves. The governing parameters are the bottom friction coefficient,  $c_d$ , the beach mean slope,  $\beta$ , and the maximum Froude number,  $F$ . In general, the spatial patterns may be quite complicated, with several unstable modes. For steep beaches with a small bottom friction coefficient, that is, for small  $R = c_d/\beta$ , the instability is very weak, perhaps negligible. Increasing  $R$  around 0.1–0.7 increases instability, which in this range gives, typically, a quite simple transverse bars pattern. A further increase in  $R$  leads to complex patterns with oblique bars, bumps and holes, and possible quasi-periodic spatial behaviour. In general, the most intense morphological activity and the most complex behaviour is found on very gently sloping beaches, for high bed roughness (large  $R$ ) and high Froude number. Wavelengths decrease with increasing  $R$ , being of the order of one to four times the width of the longshore current, close to four times for the most common values of  $R$  in natural beaches. For the dominant mode, the  $e$ -folding time is between one-third to one times the period and sand waves may therefore grow significantly while they migrate one wavelength.

In order to test the presence of this instability mechanism for field and laboratory conditions, it should be kept in mind that the observed topography may be a result of many nonlinear interacting mechanisms and it is very difficult to assess which was the driving one for the initial growth. For instance, bed-flow instability for wave driven longshore currents

is inseparable from bed-surf instability, that is, the instability stemming from the positive feedback between bottom disturbances and the disturbances in the incoming wave field. Moreover, infragravity edge wave activity has proved to be very often correlated to rhythmic topography. In spite of this difficulty, the comparison of the model prediction of sand wave initial growth with field and laboratory observations are encouraging. First, the ratio wavelength to surf zone width is in the correct order of 1.5–8, very close to the mean value, 3–4. The migrational speed is inversely proportional to the wavelength, in rough accordance with experimental data. The growth time is proportional to the squared wavelength, so that the largest features grow much more slowly than the smaller ones. In agreement with experimental observations, the model predicts that sand wave growth increases with the angle of wave incidence, and it is suggested that the maximum growth would correspond to some intermediate value between high and low incoming wave activity. Typical growth times of a sand wave train with a wavelength of 100 m are of the order of 1 day, depending on the sediment transport rate. This is not in disagreement with the available field data. Application of the model to a laboratory experiment in which a sand wave train with a wavelength of 3 m was generated yielded a growth time of 4 h, in close agreement with observations.

Intriguingly, available field studies relate rhythmic patterns with accretion beach states and beach profiles above equilibrium profile, that is, when  $R$  is expected to be high and thereby the morphological activity due to the bed-flow mechanism more intense and complex. There is some controversy regarding the orientation of the crests of sand waves. According to observations, the bars may be normal or oblique. In the latter case, they are downcurrent skewed. However, the theory predicts downcurrent or upcurrent orientation depending upon the model. The present model yields transverse crests for low  $R$  and downflow rotated crests for high  $R$ . Anyway, it seems that bar orientation is very sensitive to the longshore current profile. Clearly, it appears that there is a need for more extensive research with a unified numerical model having the capability to select any one of the individual instability mechanisms or all of them together, to choose between several sediment transport models and to use alternatively regular or irregular incoming waves. Curiously, some of the sand wave patterns are reminiscent of the spatial distribution of shear waves stemming from shear instability of the longshore current. Even though the timescales for both instabilities are very different, an investigation of the possible interaction between the two is also worthy of future research.

*Acknowledgements*—We would like to thank H. E. De Swart for the helpful and encouraging discussions concerning this work. The present research has been funded by the Spanish government, DGYCIT, under grant PB91-0594.

## REFERENCES

- Aagaard T. (1991) Multiple-bar morphodynamics and its relation to low-frequency edge waves. *Journal of Coastal Research*, 7 (3), 801–813.
- Barcilon A. I. and J. P. Lau (1973) A model for formation of transverse bars. *Journal of Geophysical Research*, 78, 2656–2664.
- Bauer B. O. and B. Greenwood (1990) Modification of a linear bar-trough system by a standing edge wave. *Marine Geology*, 92, 177–204.
- Bowen A. J. (1969) Rip currents 1. Theoretical investigations. *Journal of Geophysical Research*, 74 (23), 5467–5478.
- Bowen A. J. and D. A. Huntley (1984) Waves, long waves and nearshore morphology. *Marine Geology*, 60, 1–13.

- Bowen A. J. and R. A. Holman (1989) Shear instabilities of the mean longshore current 1. Theory. *Journal of Geophysical Research*, **94** (C12), 18023–18030.
- Bowen A. J. and D. L. Inman (1969) Rip currents 2. Laboratory and field observations. *Journal of Geophysical Research*, **74** (23), 5479–5490.
- Bowen A. J. and D. L. Inman (1971) Edge waves and crescentic bars. *Journal of Geophysical Research*, **76**, 8662–8671.
- Canuto C., M. Y. Hussaini, A. Quarteroni and T. A. Zang (1988) Spectral methods in fluid dynamics. Springer-Verlag, Berlin.
- Chappell J. and I. G. Eliot (1979) Surf-beach dynamics in time and space—An Australian case study, and elements of a predictive model. *Marine Geology*, **32**, 231–250.
- Christensen E. D., R. Deigaard and J. Fredsoe (1995) Sea bed stability on a long straight coast. *Proceedings of the 24th International Conference on Coastal Engineering*, A.S.C.E., New York, 1865–1879.
- Dalrymple R. A. (1975) A mechanism for rip current generation on an open coast. *Journal of Geophysical Research*, **80** (24), 3485–3487.
- Dalrymple R. A. and G. A. Lanan (1976) Beach cusps formed by intersecting waves. *Geology Society of America Bulletin*, **87**, 57–60.
- Evans O. F. (1938) The classification and origin of beach cusps. *Journal of Geology*, **46**, 615–627.
- Evans O. F. (1939) Mass transportation of sediments on subaqueous terraces. *Journal of Geology*, **47**, 324–334.
- Falqués A. (1989) Formación de topografía rítmica en el Delta del Ebro. *Rev. Geofísica*, **45**, 143–156.
- Falqués A. (1991) A note on the Barcelon and Lau model for transverse bars. *Rev. Geofísica*, **47**, 191–195.
- Falqués A. and V. Iranzo (1992) Edge waves on a longshore shear flow. *Physics Fluids A*, **4** (10), 2169–2190.
- Falqués A. and V. Iranzo (1994) Numerical simulation of vorticity waves in the nearshore. *Journal of Geophysical Research*, **99** (C1), 825–841.
- Falqués A., V. Iranzo and M. Caballería (1995) Shear instability of the longshore current: effects of dissipation and nonlinearity. *Proceedings of the 24th International Conference on Coastal Engineering*, 1983–1997 A.S.C.E., New York.
- Falqués A., V. Iranzo and A. Montoto (1993) Resonance of longshore currents under topographic forcing. *Physics Fluids A*, **5** (12), 3071–3084.
- Guza R. T. and A. J. Bowen (1975) The resonant instabilities of long waves obliquely incident on a beach. *Journal of Geophysical Research*, **80**, 4529–4534.
- Hino M. (1975) Theory on formation of rip-current and cuspidal coast. *Proceedings of the 14th International Coastal Engineering Conference*, A.S.C.E., New York, 901–919.
- Holman R. A. and A. Bowen (1982) Bars, bumps and holes: models for the generation of complex beach topography. *Journal of Geophysical Research*, **87** (C1), 457–468.
- Horikawa K. (ed.) (1988) *Nearshore Dynamics and Coastal Processes*, University of Tokyo Press, Tokyo.
- Hunter R. E., H. E. Clifton and R. L. Phillips (1979) Depositional processes, sedimentary structures, and predicted vertical sequences in bared nearshore systems, southern Oregon coast. *Journal of Sediment Petrology*, **49** (3), 711–726.
- Huntley D. A. (1988) Evidence for phase coupling between edge wave modes. *Journal of Geophysical Research*, **93** (C10), 12393–12408.
- Huntley D. A. and A. D. Short (1992) On the spacing between observed rip currents. *Coastal Engineering*, **17**, 211–225.
- Inman D. L., M. H. S. Elwany, A. A. Khafagy and A. Golik (1993) Nile Delta profiles and migrating sand blankets. *Proceedings of the 23rd International Conference on Coastal Engineering*, A.S.C.E., New York, 3273–3284.
- Iranzo V. and A. Falqués (1992) Some spectral approximations for differential equations in unbounded domains. *Computer Methods Applied Mechanics and Engineering*, **98**, 105–126.
- Lippmann T. C. and R. A. Holman (1990) The spatial and temporal variability of sand bar morphology. *Journal of Geophysical Research*, **95** (C7), 11575–11590.
- Miller C. and A. Barcelon (1978) Hydrodynamic instability in the surf zone as a mechanism for the formation of horizontal gyres. *Journal of Geophysical Research*, **83** (C8), 4107–4116.
- Niedoroda A. W. and W. F. Tanner (1970) Preliminary study of transverse bars. *Marine Geology*, **9**, 41–62.
- Oltman-Shay J., P. A. Howd and W. A. Birkemeier, (1989) Shear instabilities of the mean longshore current 2. Field observations. *Journal of Geophysical Research*, **94**, C12, 18031–18042.
- Osborne P. D. and C. E. Vincent (1993) Timescales of bed response in a low energy surf zone. *Proceedings of the 23rd International Conference on Coastal Engineering*, A.S.C.E., New York, 2321–2331.

- Reniers A., J. A. Battjes, A. Falqués and D. A. Huntley (submitted) A laboratory study on the shear instability of longshore currents. *Journal of Geophysical Research*.
- van Rijn L. C. (1989) *Handbook of Sediment Transport by Currents and Waves*, Delft Hydraulics, Delft, The Netherlands.
- Sasaki T. and K. Horikawa (1975) Nearshore current system on a gently sloping bottom. *Coastal Engineering in Japan*, **18**, 123–142.
- Schäffer H. A. (1994) Edge wave forced by short-wave groups. *Journal of Fluid Mechanics*, **259**, 125–148.
- Schielen R., A. Doelman and H. E. De Swart (1993) On the dynamics of free bars in straight channels. *Journal of Fluid Mechanics*, **252**, 325–356.
- Short A. D. (1992) Netherlands coast: processes, morphology and structural impacts in a storm driven multi-bar system. *Marine Geology*, **107**, 103–137
- Sonu C. J. (1969) Collective movement of sediment in littoral environment. *Proceedings of the 11th International Conference on Coastal Engineering*, A.S.C.E., New York, 373–400.
- Sonu C. J. (1973) Three-dimensional beach changes. *Journal of Geology*, **81**, 42–64.
- Van de Meene J. W. H. (1994) The shoreface-connected ridges along the central Dutch coast. *Netherlands Geographical Studies* 174, Utrecht University, Utrecht.
- Wright L. D. and A. D. Short (1984) Morphodynamic variability of surf zones and beaches: a synthesis. *Marine Geology*, **56**, 93–118.
- Wright L. D., P. Nielsen, N. C. Shi and J. H. List (1986) Morphodynamics of a bar-through surf zone. *Marine Geology*, **70**, 251–285.
- Wright L. D., B. G. Thom and J. Chappell (1978) Morphodynamic variability of high-energy beaches. *Proceedings of the 16th International Conference on Coastal Engineering*, A.S.C.E., New York.

## APPENDIX A

### NUMERICAL METHOD

The method is based upon truncated expansions in Chebyshev polynomials, a map from  $[0, \infty)$  to  $[-1, 1)$  and a collocation procedure. In order to briefly describe its application to the eigenproblem (equation 23) we will consider the simpler equation

$$a(x)\frac{d^2u}{dx^2} + b(x)\frac{du}{dx} + c(x)u = \lambda u, \quad x \in (0, \infty) \quad (\text{A1})$$

with boundary conditions  $u(0) = 0$ ,  $u(\infty) = 0$ , where  $\lambda$  is an eigenvalue and  $u(x)$  its eigenfunction. This simple equation is used instead of equation (23) in order to avoid unnecessary complications. The first step is to consider the rational map from our domain,  $[0, \infty)$ , into the  $[-1, 1)$  interval given by:

$$x = \phi(\xi) = l\frac{1 + \xi}{1 - \xi} \quad \xi \in (-1, 1) \quad (\text{A2})$$

where  $l$  is a parameter which will be specified later on. The second step is to replace each unknown function by its expansion:

$$u(x) = \sum_{n=0}^N \hat{u}_n T_n(\xi) = \sum_{n=0}^N \hat{u}_n T_n(\phi_2^{-1}(x)) \quad x \in (0, \infty) \quad (\text{A3})$$

where  $T_n(\xi) = \cos(n \cos^{-1}\xi)$  are the Chebyshev polynomials. Then, the Gauss-Lobatto nodes

$$\xi_i = \cos \frac{\pi i}{N} \quad i = 0 \dots N \quad (\text{A4})$$

transformed into:

$$x_i = \phi(\xi_{N-i}), \quad i = 0 \dots N - 1 \tag{A5}$$

are considered. Notice that  $x_0 = 0$  and  $x_N = \infty$ . The  $l$  parameter is the distance from  $x = 0$  where there are half the discretization nodes. This makes it possible to control the mesh density, so that small values give a high density near  $x = 0$ , whereas large values expand the mesh. The suitable values depend on the problem we are solving. In the case of our morphodynamical model they are of the order of the longshore current width. The first and second order derivatives of any function,  $u(x)$ , are computed by means of the  $D, D^2$  matrices:

$$\left. \frac{du(x)}{dx} \right|_{x=x_j} = \sum_{k=0}^{N-1} D_{jk} u_k \quad j = 0 \dots N - 1 \tag{A6}$$

$$\left. \frac{d^2u(x)}{dx^2} \right|_{x=x_j} = \sum_{k=0}^{N-1} D_{jk}^2 u_k \quad j = 0 \dots N - 1 \tag{A7}$$

where  $u_k = u(x_k)$ . In order that these formulae be applicable the function must vanish at infinity so that the  $x_N$  node has not to be taken into account. By means of the chain rule the following expressions for  $D, D^2$  can be obtained:

$$(D)_{jk} = \frac{1}{\phi'(\xi_j)} \bar{D}_{jk} \quad (D^2)_{jk} = \frac{1}{\phi'(\xi_j)^2} (\bar{D}^2)_{jk} - \frac{\phi''(\xi_j)}{\phi'(\xi_j)^3} \bar{D}_{jk}, \quad j, k = 0 \dots N - 1 \tag{A8}$$

where  $\bar{D}$  and  $\bar{D}^2$  are the Chebyshev derivative operators, which can easily be obtained from the derivatives of Chebyshev polynomials (Canuto *et al.*, 1988, p. 69). Finally, following a collocation procedure, the eigenproblem (A1) is replaced by its discretized version

$$a(x_j) \sum_{k=0}^{N-1} D_{jk}^2 u_k + b(x_j) \sum_{k=0}^{N-1} D_{jk} u_k + c(x_j) u_j = \lambda u_j, \quad j = 1 \dots N - 1 \tag{A9}$$

$$u_0 = 0.$$

The boundary condition at infinity,  $u(\infty) = 0$ , has been implicitly included simply by dropping the  $x_N$  node.

Equation (23) of our morphodynamical model has been discretized in the same way as has been shown for equation (A1), and the numerical problem has been solved by a standard eigenvalue computation subroutine.

This spectral numerical technique has proved to have much higher resolution than the more traditional finite difference methods, and it has been applied efficiently to edge wave and shear wave computation. It can be applied to nonlinear problems as well (Falqués *et al.*, 1995). The details can be seen in Falqués *et al.* (1993) or Iranzo and Falqués (1992). Some additional information on the numerical solution of similar eigenproblems may be found in Falqués and Iranzo (1994). The book by Canuto *et al.* (1988) provides a valuable general overview of numerical spectral methods applied to fluid mechanics.